Geosystems and Geoenvironment 2 (2023) 100120

Contents lists available at ScienceDirect

Geosystems and Geoenvironment

journal homepage: www.elsevier.com/locate/geogeo

Development and testing a low-cost device for airborne PM monitoring in highly anthropized areas: The international maritime hub of Civitavecchia (Rome, Italy)

Federico Lucci[a,*], Giancarlo Della Ventura[b,c,d], Daniele Piazzolla[e,f], Carlo Venettacci[b], Andrea Terribili[e,f], Cecilia La Bella[b], Alessandra Conte[b,c], Simone Bonamano[e,f], Sergio Scanu[e,f], Francesco Radica[c,g], Marco Marcelli[e,f]

[a] Dip. Scienze della Terra e Geoambientali, Università Degli Studi di Bari "Aldo Moro", Via E. Orabona 4, Bari 70125, Italy
[b] Dip. Scienze, Università di Roma Tre, L. S. Leonardo Murialdo 1, Rome 00146, Italy
[c] INFN-LNF, Via E. Fermi 40, Frascati, Rome 00044, Italy
[d] INGV, Via di Vigna Murata 605, Rome 00143, Italy
[e] Ocean Predictions and Applications Division, Centro Euro-Mediterraneo sui Cambiamenti Climatici, Italy
[f] Laboratory of Experimental Oceanology and Marine Ecology, Department of Ecological and Biological Science (DEB), Università degli Studi della Tuscia, Civitavecchia, Italy
[g] Dip. Di Ingegneria e Geologia, Università degli Studi "G. d'Annunzio" Chieti-Pescata, Pescara, Chieti, Italy

ARTICLE INFO

Article history:
Received 15 April 2022
Revised 6 July 2022
Accepted 5 August 2022

Handling Editor: Xiaofang He

Keywords:
Air quality monitoring
Particulate matter
Port emissions
Black carbon
Low-cost device
COVID-19
Airborne microplastics

ABSTRACT

In this paper we describe our work aimed at designing a system able to measure the particulate matter (PM) concentrations via an optical particle counter (OPC) and simultaneously collect it via standard 2.5 cm filters for laboratory characterization. The Port of Civitavecchia (Italy), one of the most important maritime hubs of the Mediterranean Sea, was selected as a test site for an eight-months monitoring campaign. Comparison between the data provided by our device with those from the referenced and certified monitoring stations from the governmental Regional Agency for the Protection of the Environment (ARPA Lazio) allowed to define clear threshold values ($PM_{10} = 25\ \mu g/m^3$ and $PM_{2.5} = 10\ \mu g/m^3$). These threshold values need to be considered when correcting the OPC raw data with respect to the humidity (RH) conditions. The sample material was characterized through optical microscopy and SEM-EDS (scanning electron microscopy coupled with energy-dispersive X-ray fluorescence) and spectroscopy (FTIR, Raman), showing a variegate composition from Al-Fe-oxides to silicates, carbonates, and sulfates, to coal and amorphous carbon together with microplastics and textile fibers. As a final test, we analyzed the PM trends provided by our device during the COVID-19 lockdown, when stringent restrictions in the human activities caused well-known fluctuations in the atmospheric pollution. We again observed an evolution of the PM peaks in excellent agreement with the results yielded by the ARPA Lazio monitoring stations. This result provides a valuable confidence test for our devices highlighting the effectiveness of the presented strategy for airborne particulate-matter monitoring.

1. Introduction

Atmospheric pollution is a major issue affecting the ecosystems (IHME, 2018), it may be of natural origin (e.g., sea salt, volcanoes, mineral dust, biogenic emissions; Mokadem et al. 2014; Silva et al. 2020; Trejos et al., 2021), but nowadays its most relevant sources are of anthropogenic origin, such as industries, transport, and energy production factories (Kumar et al., 2014). The growing of urbanization and the related human activities requires an intense energy consumption, and, as a result, a variety of pollutants such as carbon monoxide (CO), nitrogen dioxide (NO_2), ozone (O_3), sulfur dioxide (SO_2), and particulate matter (PM) are released into the atmosphere negatively affecting all ecosystems, the health of organisms and human health (e.g., Piazzolla et al., 2021).

Highly populated areas, such as metropolitan and industrial districts, are often not capable to match the air pollutant emission

* Corresponding author.
E-mail address: federico.lucci@uniba.it (F. Lucci).

https://doi.org/10.1016/j.geogeo.2022.100120

standards (Kumar et al., 2021; Li et al., 2018). Considering that 40–45% of the world's population lives within 100–150 km from the seashore, hence the coastal anthropized areas act as major pollution hot spots (Cole et al., 2011). This problem is particularly evident where maritime hubs are: 25% of the overall world energy consumption is due to transport, and over 80% of world trade is maritime (Gobbi et al., 2020 and references therein).

The pollutants released in the atmosphere can enter the marine environments through wet and dry fallout (Bunzl et al., 1984) directly into the sea or through river solid load, consequently generating toxic effect on living organisms (including humans) through bioaccumulation and biomagnification processes (Scanu et al., 2015; Kumar et al., 2021; De Nazelle et al., 2017). Consequently, this implies, directly and indirectly, an increasing rate of human disease and death (Kumar et al., 2021).

According to the European Environment Agency Air Quality Report 2020 (EEA Report No. 9/2020), among the whole air pollutants exceeding worldwide emission standards, the particulate matter (PM) has the most severe impact on health (Brunekreef and Forsberg, 2005; Minguillón et al., 2012; Zhang et al., 2018) and on ecosystems (Grantz et al., 2003; Zhang et al., 2018). The PM is a mixture of suspended particles with a nominal average diameter <10 μm and it is further clustered through the aerodynamic diameter in PM_1 (<1 μm), $PM_{2.5}$ (<2.5 μm) an PM_{10} (<10 μm), respectively (Agrawal et al., 2021). The term of PM also includes droplets with diameter <10 μm. Volcanic eruptions, dust storms, forest fires, and sea spray are the natural sources of PM; fossil fuel combustion and industrial activities are instead the main anthropogenic sources of PM pollution (Gozzi et al., 2017).

The PM concentration depends on many factors; a key-role is played by (i) the sources, (ii) the regional background (i.e., natural vs. anthropogenic PM) and (iii) the atmospheric conditions (Minguillón et al., 2012). Overall, the latter (e.g., wind speed and direction, rain, temperature, and relative humidity) have a strong effect in directly influencing diffusion, dilution, accumulation, and removal of air pollutants in a specific area (Kamińska, 2018; Hu et al., 2021), also controlling the PM concentration at the very local scale (Kavak Akpinar et al., 2006).

The concentrations of $PM_{2.5}$ and PM_{10} associated with environmental hazard are regulated by European emission standards (Directive 2008/50/EC). Accordingly, the annual threshold is 25 $\mu g/m^3$ for $PM_{2.5}$ while being 40 $\mu g/m^3$ for PM_{10}; a daily limit of 50 $\mu g/m^3$ should not been exceeded more than 35 times (days) per year.

Despite the development of innovative air quality monitoring technologies (Gozzi et al., 2015, 2017 and references therein), the air pollution is still a relevant issue needing a better comprehension of the airborne pollutants' behaviors and characteristics (Gozzi et al., 2015, 2017; Van den Bossche et al., 2015; Khaniabadi et al., 2018; Soggiu et al., 2020). Even if the existing official and certified networks based on static stations are capable to produce reliable data, their high costs do not permit to develop a satisfactory and up-to-date spatial and temporal analysis of airborne PM (Peters et al., 2013; Gozzi et al., 2015; Thompson, 2016; Jerrett et al., 2017). Therefore, there is the need of novel monitoring networks based on smart, compact, portable, and, above all, low-cost devices to generate a spatial-dense, reliable, and real-time monitoring of the airborne pollutant (Gozzi et al., 2015).

In this work, we present the results of an eight-month PM measurement campaign within the major maritime hub of Port of Civitavecchia (northern to Rome, Italy; Fig. 1). The main aim was the test of a newly designed low-cost (ca. 1000 €) device equipped with an OPC (optical particle counter) sensor able to measure but simultaneously collect the airborne material for later laboratory studies. The raw data are statistically evaluated and discussed in comparison with the referenced and certified data from the (few) air quality monitoring stations from the ARPA Lazio network installed in the same area. This calibration allowed us to evaluate the performance of the OPC as a function of the hygroscopicity conditions (Crilley et al., 2018) and explore the effectiveness of the statistical approach based upon the k-Köhler theory (Petters and Kreidenweis, 2007) to derive the corrected dry mass. Lastly, we verified the capability of our device to monitor extremely variable events of anthropic PM production such as those expected at the end of the Italian hard lockdown because of the COVID-19 pandemic.

2. Materials and methods

2.1. Air pollution monitoring site

The municipality of Civitavecchia with a stable population of ca. 50 K inhabitants belongs to the Metropolitan City of Rome Capital (Latium, Italy) since the 1st of January 2015. It is located on the eastern Tyrrhenian Sea, 70 km north to the city center of Rome and less than 50 km north to the Rome-Fiumicino International Airport "Leonardo da Vinci" (IATA airport code: FCO) with the latter one classified as one of the 50th busiest international airports with more than 49 M passengers per year prior to the COVID-19 pandemic (official data at December 2019; https://www.adr.it/). The municipality of Civitavecchia hosts the Port of Civitavecchia (also known as "Port of Rome") representing one of the most important Italian hubs for the maritime transport. It is also part of the "Motorway of the Sea of the south-west Europe" (Fig. 1a). The Port extends to the NW of the city of Civitavecchia (Fig. 1b) and is characterized by the presence of regular ("Ro-Ro") and cargo ferry piers and also carrier ship docks. It also hosts the Rome Cruise Terminal, making this port one of the main hubs for Mediterranean Cruise tourism (Bonamano et al., 2017; Cafaro et al., 2018; Martellucci et al., 2021). The Port of Civitavecchia, together with the FCO airport, constitutes also one of the most important touristic and commercial hub system of the southern Europe and of the whole Mediterranean region.

The municipality of Civitavecchia is also characterized by the presence of the following national strategic structures: the gas-fueled combined-cycle Tirreno Power Station (TPS) and the coal-fired ENEL Torrevaldaliga Nord Power Station (TVN; Piazzolla et al., 2020a, 2020b; Gobbi et al., 2020). Both these power plants are located at the NW termination of the Port area (Fig. 1b). Lastly, the Port of Civitavecchia, the FCO Airport and the city of Rome are connected via the highway system belonging to the European Route "E80" (Supplementary Data, Fig. S1).

It is worth noting that the air quality of the municipality of Civitavecchia is currently monitored only by nine static stations (Fig. 1b) belonging to the governmental Regional Agency for the Protection of the Environment (Agenzia Regionale per la Protezione Ambientale – ARPA). Five stations are from the ARPA Lazio: (i) station n°15 "Civitavecchia" in the city center (linear distance from the low-cost device, hereafter "distance", ca. 1.4 km), (ii) station n°60 "Porto" at the southern "Varco Vespucci" access to the port area(distance ca. 0.3 km), (iii) station n°83 "Villa Albani" located north to the city center (distance 0.6 km), (iv) station n°84 "Via Morandi" southern to the city center (distance ca. 1.9 km), and (v) station n°85 "Via Roma" close to the city center (distance 0.75 km). Since the month of May 2016, eleven stations from the former ENEL (Ente Nazionale per l'Energia Elettrica) monitoring network are managed by the ARPA Lazio. Four of these latter stations are within the area of interest and they are: (i) station n°103 "Fiumaretta", close to the port (distance ca. 0.83 km), (ii) station n°104 "Faro", in the eastern and upper part of the city town (distance ca. 2.6 km), (iii) station n°105 "Campo Oro", southern to "Via Morandi" station (distance ca. 2.4 km), and (iv) station n°106 "S. Gordiano", southern to the Civitavecchia town (distance ca. 3.4 km).

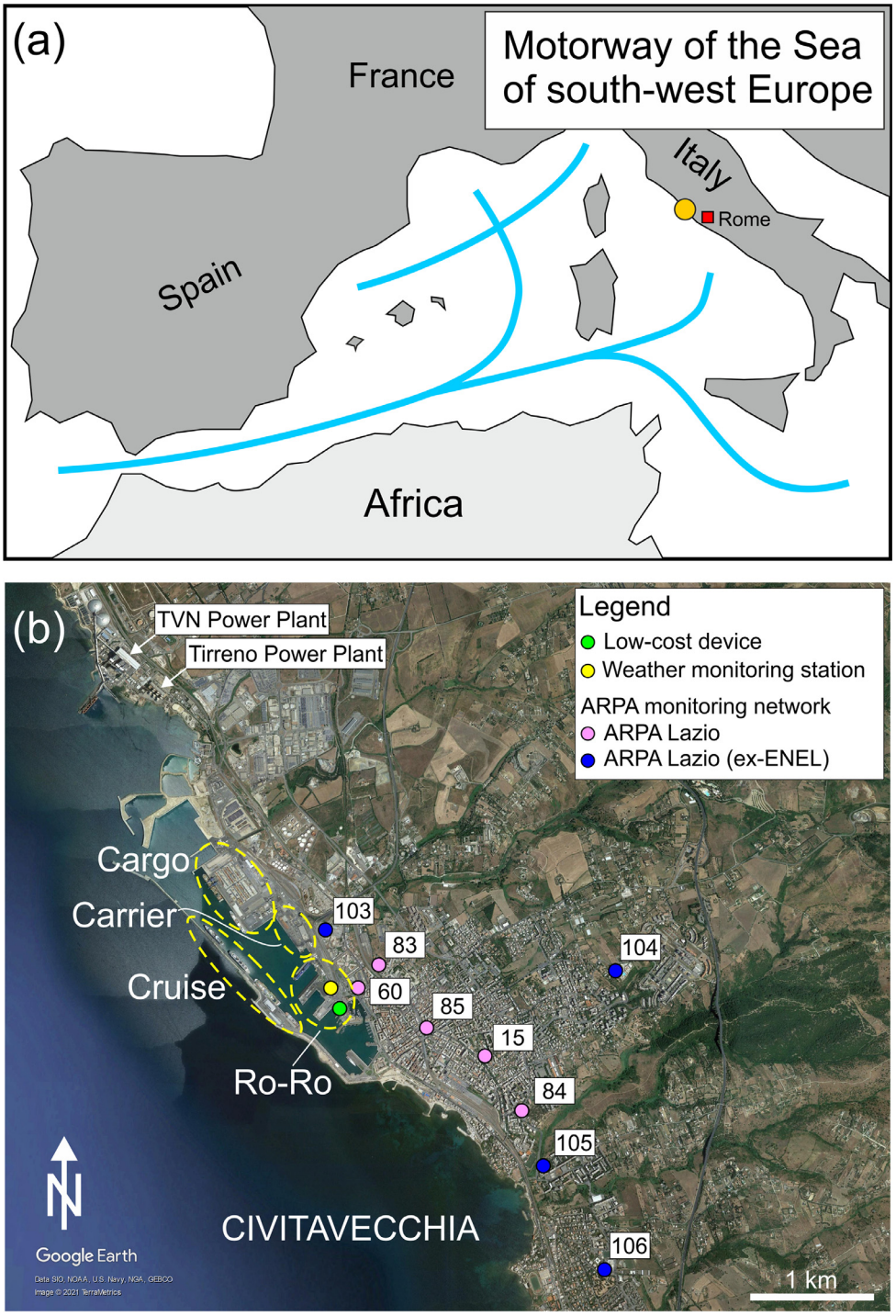

Fig. 1. (a) Simplified map of the western Mediterranean Sea; the EU "Motorway of the Sea of South-West Europe" (e.g., Papadimitriou et al., 2018) are indicated in cyan and the location of the Civitavecchia maritime hub is the yellow square. (b) Satellite image of the Port and Municipality of Civitavecchia (Image 2021 TerraMetrics from Google Earth Pro, Data SIO, NOAA, U.S. Navy, NGA, GEBCO; courtesy of Google) with mooring piers by ship category and location of the governmental ARPA Lazio (red dots) and ARPA Lazio Ex-ENEL (blue dots) air quality monitoring stations indicated. The weather monitoring station (yellow dot) and the site of installation of the tested low-cost device (green dot) are also indicated. The location north to the Port of the two TVN and Tirreno power plants is also reported in Fig. 1b.

The setting of the Port of Civitavecchia clearly represents a valuable target area for monitoring the anthropogenic PM and for the development and testing a new device that could also implement the existing low-density nodes air quality monitoring governmental network.

The system tested during this study was installed on the roof of the Laboratory of Experimental Oceanology and Marine Ecology (LOSEM; University of Tuscia, Viterbo, Italy) building which is located in the southern area of the Port, close to the ARPA Lazio station n°60 "Porto", to a certified weather monitoring station and also to the city center of Civitavecchia.

2.2. PM monitoring set-up

A PM monitoring campaign, from December 2019 to August 2020, was developed based on the original low-cost device pre-

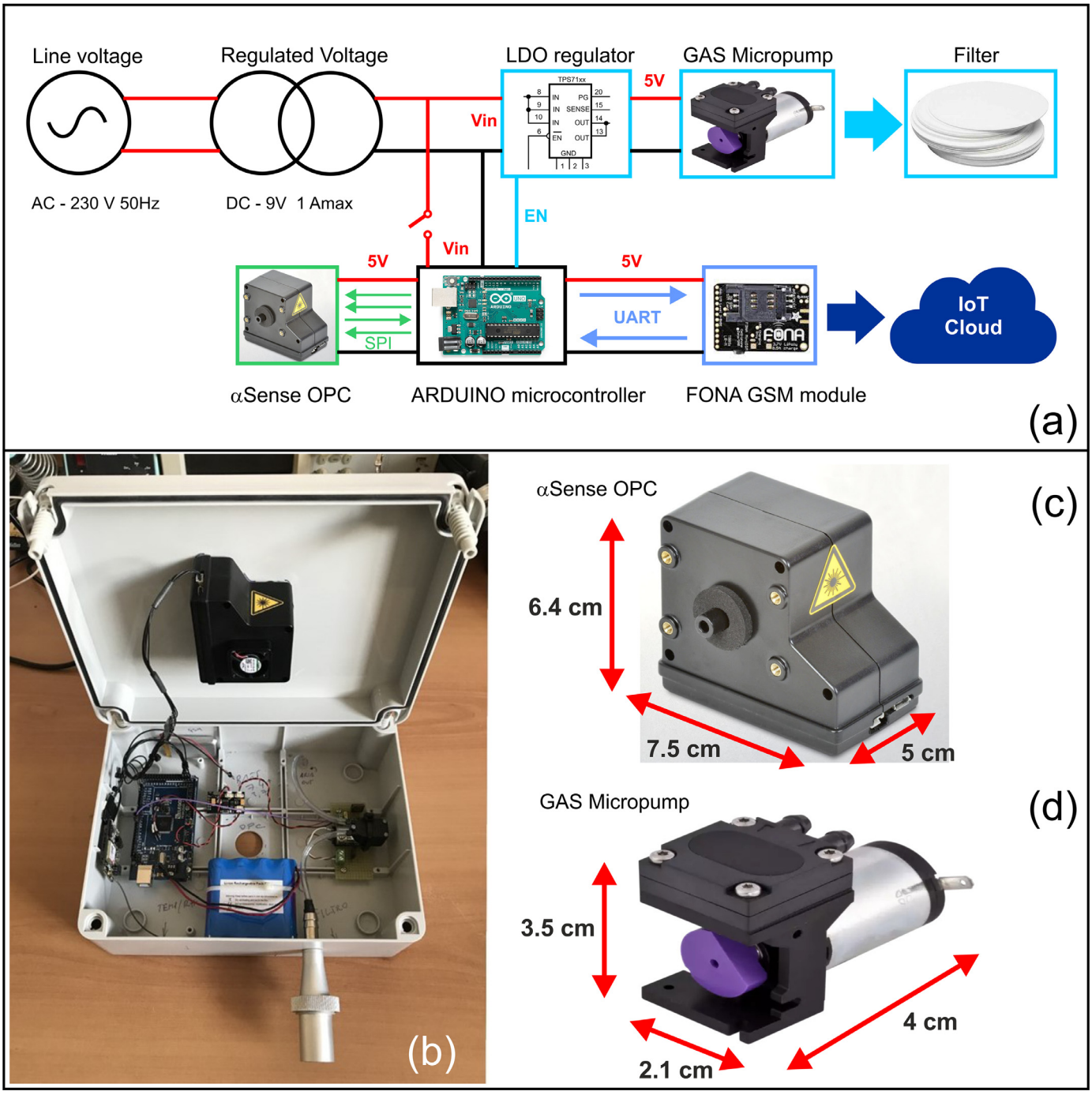

Fig. 2. (a) Simplified scheme of the device presented in this work. (b) The assembled OPC-equipped low-cost system. (c) The AlphaSense© optical particle counter OPC–N3 and (d) the Micro Diaphragm Gas Pump used.

viously presented and tested by Gozzi et al. (2015, 2017) (Fig. 2) and designed to be transportable and easily implementable with further additional sensors. As shown schematically in Fig. 2a, the device (Fig. 2b) is powered by an AC/DC power supply and uses an Arduino board, equipped with an ATmega microcontroller for the sensors management and data transfer. The PM sensor is an Optical Particle Counter (OPC–N3) manufactured and certified by AlphaSense® (Fig. 2c), which is able to quantitatively measure PM_1, $PM_{2.5}$ and PM_{10} concentrations in real-time using a LASER interferometry system, and to provide the airborne microparticles size and mass/air volume. Data transfer is carried out via the SPI (Serial Peripheral Interface) protocol, through a 4-logic signals. Moreover, our designed system is connected to an IoT cloud server, through an integrated GSM module equipped with an UART (Universal Asynchronous Receiver-Transmitter) interface, in order to access the data remotely from any personal computer or smartphone, without the need of an external memory. The device used here has been also equipped for the first time with an additional set-up to collect the particulate, consisting of a micro-pumping and a filtering system able to sample in real-time PM $>$ 0.4 mm (Della Ventura et al., 2017). The activation of the Micro Diaphragm Gas Pump (Fig. 2d), at predefined time intervals, is managed by

a digital output of the Arduino board through a Low-DropOut (LDO) voltage regulator. The filters can be easily removed at desired intervals to be transferred to the laboratory for further microscopic and chemical analyses. This sampling set-up represents the main novelty and innovation of our device with respect to traditional monitoring stations used by governmental agencies such as the ARPA Lazio, as well as other available commercial low-cost systems. In fact, in environmental pollution assessment studies, it is crucial to be able to characterize, besides the amount, also the typology (morphology and composition) of solid pollutants (Kgabi et al., 2008; Adachi et al., 2010; Zeb et al., 2018; Dong et al., 2018, 2019). This information is essential to identify the source(s) of the airborne pollution and to develop effective environmental protection strategies. The instrument, for the development and testing campaign, was connected to the mains electricity allowing therefore a continuous operating time without standby when working. The system was set on voltage range of 4.8 to 5.2 VDC as required by the OPC–N3 counter. The OPC–N3 operating parameters were measurement mode 180 mA, digital interface SPI (Mode1) via USB, particle range 0.35 to 40 mm with 24 bins size categorization, total flow rate of 5.5 L/min and maximum particle count rate of 10 K particles/second. Furthermore, the operativity of the Arduino board is factory-certified for air temperature in the range −40 to 85 °C, whereas the AlphaSense® OPC–N3 counter is factory-certified for temperature ranging −10 to 50 °C. Moreover, the OPC–N3 counter is certified also for RH in the range 0–95%. No specifications are given for oxygen content in air.

During the test campaign, the PM concentrations were monitored at intervals of ten minutes, whereas sampling filters (glass fiber filters, 25 mm in diameter and 0.7 μm mesh) were weekly collected (with a frequency ranging from 2 to 7 days). The number of particles measured by the OPC in each dimensional class was automatically converted into $\mu g/m^3$ of air through a built-in factory-determined calibration routine (Crilley et al., 2018) and certified by AlphaSense®. The hourly average PM_1, $PM_{2.5}$, and PM_{10} concentrations are reported in Supplementary Data, Table S1. The daily average concentrations of PM_1, $PM_{2.5}$, and PM_{10} classes were calculated (Supplementary Data, Table S2) in order to compare the raw data with respect to the available certified daily data from the governmental ARPA Lazio monitoring network (http://www.arpalazio.net/main/aria/sci/basedati/chimici/chimici.php).

2.3. PM morphological characterization

The sampling filters were preliminary examined with an optical stereoscopic microscope. Selected microparticles extracted from the filters were characterized by combining optical and scanning electron microscopy (SEM; SNE3200M Table top SEM by SEC, Korea), and Raman (Horiba; Japan) and Fourier Transform Infrared (FT-IR; Bruker, USA) spectroscopies. Analyses were done at DAFNE-L (Istituto Nazionale di Fisica Nucleare, INFN) in Frascati (Rome, Italy). The SEM investigations were developed using a SNE3200M microscope, equipped with a high-resolution energy-dispersive (EDS) Bruker detector (XFLASH Detector 410 M) and the ESPRIT 1.9 software. The micro-FT-IR spectra were collected using a Bruker Hyperion 3000 microscope attached to a Vertex V70 optical bench. A quartz source was used for the IR beam, coupled with a KBr beam-splitter and a mercury-cadmium-telluride (MCT) detector for measurements both in the medium IR (MIR) and in the near IR (NIR). The Raman spectra were acquired using a Horiba NRS-5100 spectrometer, equipped with a 532 nm green laser. Spectroscopic data were then compared with the open-source database Open Specy (Cowger et al., 2021) for a proper identification of the analyzed compounds.

2.4. Meteorological background

Modeling how and where the air pollutants are transported within a specific area requires the knowledge of the local variability of the weather conditions (or meteorological background). This being the case, in the following we discuss the PM concentration with respect to the wind parameters (i.e., speed and direction) and to the relative humidity (RH) as measured by the Civitavecchia Coastal Environment Monitoring System (C–CEMS; Bonamano et al., 2016). Wind speeds data were expressed in m/s whereas wind directions were in °N, whereas RH is expressed in 0–100% scale (Supplementary Data, Table S3).

Concerning air temperature, Horemans et al. (2011) demonstrated a low correlation between PM and daily temperatures in the Alhambra locality in Spain. Furthermore, Elminir (2005) demonstrated only an interesting positive relationship between ambient air temperature and O_3 and NO_2 pollutants, whereas a weak to insignificant relationship between the air temperature and the primary pollutants. Consequently, we decided to focus here only on wind characteristics and RH, which represent, for the study area, the most relevant weather variables. However, as outlined by Gao et al. (2019), the daily temperature could affect the PM background value. Therefore, we believe that temperature is not relevant at this stage of development in the selected Mediterranean coastal area, but it will certainly become of high interest when the device will be tested in continental areas and/or mountain environments.

2.5. Workflow for the analysis of variance

To evaluate the discrepancy between the low-cost device and the selected ARPA Lazio referenced stations, we developed in this study a classic and widely applied analysis of variance (ANOVA; Piras et al., 2013). This procedure is based on the evaluation of the existing relationship between the correlation coefficients ("Multiple *R*", or "*R*") and the coefficients of determination ("R^2") from the regression analysis applied to the PM contents from each ARPA station with respect to the PM values measured from the tested OPC–N3, considered as the differentiation index or the independent variable. In this approach *R* values indicate the strength and direction of a linear relationship between data, with *R* ranging from −1 to 1, where $R = -1$ indicating a strong negative relationship, $R = 1$ a strong positive relationship and $R = 0$ indicating no relationship at all. The R^2 indicates the proportion of variance that is expressed by the independent variable (i.e., the differentiation index), with R^2 ranging from 0 to 1, where $R^2 = 1$ indicates that the model perfectly fits all the data.

Significance *F*-test has been produced for each regression analysis. It represents the probability of lack of significance of the regression model. Considering a conventionally defined level of significance equal to 0.05, regression models are accepted for *F*-test values < 0.05. The regression analysis was performed using the Regression Tool of the Analysis ToolPak in Microsoft Excel 2019.

2.6. Workflow for the PM correction

As previously discussed by Crilley et al. (2018, 2020), the OPC data must be corrected for ambient RH to allow comparisons with particle mass referenced instruments. Following the method proposed by Crilley et al. (2018, 2020), we produced an OPC-measured PM correction to ambient RH with respect to the nearest (ca. 0.3 km) ARPA Lazio referenced station n°60 "Porto". Unfortunately, this referenced instrument, for the time-interval of interest, did not provided $PM_{2.5}$ data, whereas the other ARPA Lazio stations were too far away (>0.5 km) from our device to be considered suitable

for the statistical analysis. Therefore, we calculated only the correction for the PM_{10} concentration measured by the OPC–N3.

The equation used (Eq. (1)) is that of Pope (2010) in the form of Eq. (5) in Crilley et al. (2018):

$$a_W = \frac{\left(\frac{m}{m_0} - 1\right)}{\left[\left(\frac{m}{m_0} - 1\right) + \left(\frac{\rho_W}{\rho_p} k\right)\right]} \quad (1)$$

where the density of water (r_w) and bulk dry particles (r_p) are assumed to be 1 g/cm^3 and 1.65 g/cm^3, respectively (Crilley et al., 2018), the water activity (a_W) is the ambient RH/100, m and m_0 are the wet (RH = measured value) and dry (RH = 0%) aerosol mass, with the latter one from the ARPA Lazio referenced station n°60 "Porto", respectively.

The relationship between particle hygroscopicity and volume is expressed by the hygroscopicity parameter k which is a quantitative measure of aerosol water uptake characteristics vs. cloud condensation nuclei activity (k-Kohler theory in Petters and Kreidenweis, 2007) and chemical composition of atmospheric aerosol particles (Wang et al., 2017 and references therein). The k parameter is here obtained through a non-linear best fit of the humidogram calculated for the m/m_0 mass ratio as a function of the water activity (a_W).

The non-linear best fitting method proposed is based on the broadly applied method of the minimization of the sum of the squared residuals (Lucci et al., 2016, 2020; Moghadam et al., 2021) of the m/m_0 vs. a_W relationship expressed by Eq. (1), using the Solver Tool of the Analysis ToolPak in Microsoft Excel 2019. The k parameter is then used to calculate the factor (C) to correct the raw OPC PM data using the following Eqs. (2) and (3):

$$C = 1 + \frac{\frac{k * \rho_W}{\rho_p}}{-1 + \frac{1}{a_W}} \quad (2)$$

$$PM_{corrected} = \frac{PM_{raw}}{C} \quad (3)$$

3. Results

3.1. Airborne PM measured concentration

Hereafter, we present the daily average PM values as obtained by the raw data from the OPC instrument. During the eight-month monitoring campaign, (i) the PM_1 measured concentration ranges 1–22 μg/m^3, with a mean value of 4 μg/m^3, (ii) the $PM_{2.5}$ values ranges 2–42 μg/m^3, with a mean concentration of 11 μg/m^3, and (iii) the PM_{10} amounts ranges 5–152 μg/m^3, with a mean value of 32 μg/m^3. Trends are graphically presented in Fig. 3. Overall, the daily average concentrations of PM_{10} are always higher than those of $PM_{2.5}$ and PM_1. The calculated mean $PM_{2.5}$ and PM_{10} concentrations never exceeded the annual European air quality standard values of 25 μg/m^3 and 40 μg/m^3 (Directive 2008/50/EC), respectively. However, the measured PM_{10} values exceeded twenty-eight times the European daily limit value of 50 μg/m^3 (Directive 2008/50/EC). At the time of writing, there are no European standard values for PM_1 concentrations.

The discontinuity of data acquisition in the period March-June 2020 is due to the stringent decrees emanated by the Italian Government to control the spread of the COVID-19 pandemic disease, making extremely difficult to access to the LOSEM building for the ordinary maintenance of the device. Other minor data gaps are caused by power supply failures and to device-maintenance.

3.2. Morpho-chemical characterization of airborne PM

The morphological classification of PM is a complex task due to the wide variability in size and shape. After a preliminary examination of the sampling filters through optical microscopy, the morphological and micro-chemical study of the PM particles (Fig. 4) was done through a scanning electron microscope (SEM) equipped with an energy dispersive spectrometer (EDS) for X-ray fluorescence analysis. At the optical microscopy scale, most of the particles shows a homogeneous blackish color suggesting the presence of carbon films coating the grains. Based on the particle shapes, two main morphological populations are identified: (i) granular particles characterized by variable sphericity and rounding degrees and (ii) non-granular particles showing elongated, fibrous and lamellar morphologies. Qualitative micro-chemical analyses revealed the presence of a wide range of compositions pointing to very heterogeneous nature of the sampled airborne PM particles. The most representative material from the whole set of collected particles consists of (i) aluminum and iron oxides (Fig. 4a,c), (ii) silicates (cf. quartz, cf. feldspar); (iii) carbonatic fragments, and (iv) C-rich (cf. coal) fragments (Fig. 4d). The presence of Ca-sulfate (cf. gypsum; Fig. 4b) and NaCl (cf. halite) is also relatively common.

Raman spectroscopy was applied to identify the nature of carbon coats on filters (inset in Fig. 4e) and particles. The obtained spectra (Fig. 4e) show intense scattering at 1600 and 1400 cm^{-1} compatible with amorphous carbon, whereas peaks at about 1100 cm^{-1} and <600 cm^{-1} are attributable to calcium-carbonate (cf. calcite) and to transitional metal oxides, respectively. Thus, from Raman scattering, most of the analyzed particles can be interpreted as multi-phase calcareous and metal fragments invariably coated by thin films of amorphous carbon.

Concerning the non-granular microparticles, and in particular the fibrous and the elongated ones (inset in Fig. 4f), those having a relative transparency with whitish, bluish and reddish colors, were analyzed through IR spectroscopy, a technique that is particularly suitable to identify organic matter (Tseng et al., 1996; Carballo et al., 2008; Wang et al., 2013). Representative FT-IR spectra are shown in Fig. 4f. Although the correct classification of these fragments is difficult due to the significant degradation and weathering associated with the coastal-marine environment, a comparative approach using the Open Specy data base (Cowger et al., 2021) allowed an identification of textile fibers, plastics, and cellulose fragments (e.g., Fig. 4f). Interestingly, the presence of widespread microplastic particles had already been identified in the coastal sediments of the same area (Piazzolla et al., 2020b) and in marine organisms sampled in the port waters (Piazzolla et al., 2020a) as well as in commercial fishes from the same area (Miccoli et al., 2022). With this work the presence of microplastics is also identified for the first time in the study area as airborne respirable materials, thus confirming their great dispersion in the whole environment as reported in previous studies of other localities (Prata, 2018; Enyoh et al., 2019; Huang et al., 2020).

4. Discussion

In the following section, we will discuss the results obtained for the airborne PM dispersion, firstly as a function of local wind-parameters and later through comparison with the data from the ARPA Lazio monitoring stations located in the municipality of Civitavecchia. A very preliminary source-to-sink approach for the C-rich material is also tentatively proposed.

Lastly, a comparison with data from the ARPA regional network is developed for the measured PM peaks during the month of May 2020, corresponding to the transition from "Phase-1″ to "Phase-2″ of the COVID-19 lockdown in Italy.

4.1. PM vs. local winds

The anthropogenic PM from highly populated areas is generated by industrial emissions, road dust, vehicle exhaust (Nel, 2005;

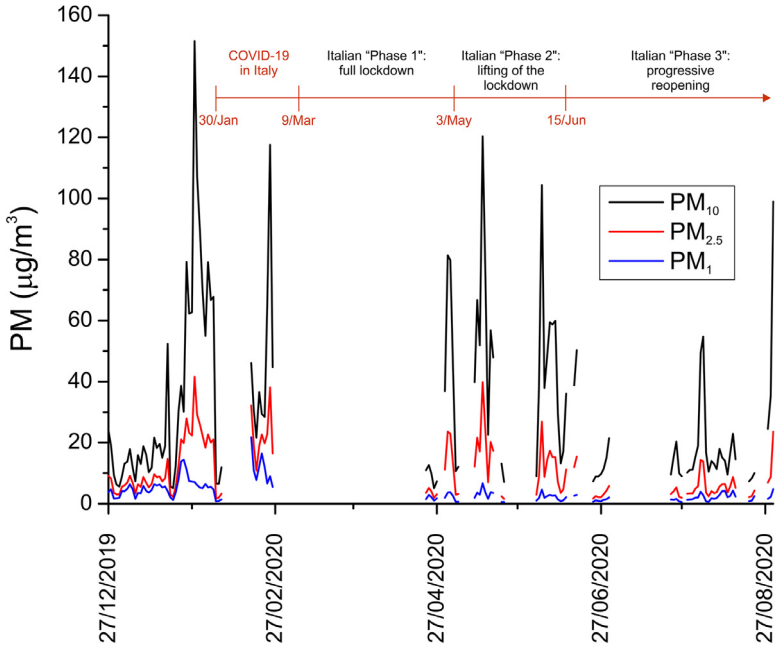

Fig. 3. Daily average uncorrected concentrations for PM_{10}, $PM_{2.5}$ and PM_1 as detected by the OPC–N3 for the whole test campaign. The dates of appearance of COVID-19 in Italy and of significant Italian Government Decrees to contrast the pandemic are indicated. Data gaps are due to COVID-19 full lockdown ("Phase-1" Decree), and to the device maintenance.

Guo et al., 2014; Brauer et al., 2016; Zhang et al., 2018) and gas-to-particle conversion processes in the atmosphere (i.e., "secondary PM"; Guo et al., 2014).

In the last two decades, many studies (Jacob and Winner, 2009; Pearce et al., 2011; Guo et al., 2014; Huang et al., 2014; Zhang et al., 2018) clearly demonstrated that the PM and the air pollutants concentration and their spatial distribution in a specific area can be strongly influenced by the meteorological background which ultimately controls their transport and accumulation. Among the many variables, many works highlighted the principal roles on PM levels exerted by precipitations and wind characteristics (Li et al., 2014; Zhang et al., 2015, 2018). Concerning the wind, a higher speed mainly affects the areal dispersion of pollutants (Tian et al., 2014; Zhang et al., 2018), whereas the direction mainly determines the source (i.e., the tipology) of pollutants in the sampled area (Guerra et al., 2006; Zhou et al., 2015).

For this study, the hourly wind speed and direction were obtained from the automatic weather station (Bonamano et al., 2016) located close to the LOSEM building where the tested device was installed (Fig. 1b). During the whole measurement campaign (Fig. 5a), except for the COVID-19 full lockdown period where no data were collected, the wind speed was in the range 0.4–14.4 m/s (average 3.3 m/s). Following the method proposed by Jenks (1967) the wind speed was classified into six levels with their relative proportions: (i) L1 <2 m/s corresponding to 29.9% of measured wind speeds, (ii) L2 2–4 m/s and 40.9%, (iii) L3 4–6 m/s and 18.5%, (iv) L4 6–8 m/s and 7.0%, (v) L5 8–10 m/s and 2.6%, and (vi) L6 >10 m/s and 1.2%. The wind directions were visualized by using four main provenance quadrants (I, II, III, and IV, respectively) and relative proportions are presented in the wind-rose diagram in Fig. 5a: (i) I is blowing from N 0–89° and corresponds to 16.8% of measured wind directions, (ii) II is from N 90–179° and 20.7%, (iii) III is from N 180–269° and 27.7% and (iv) IV is from N 270–359° and 34.6%. The wind data indicates that, during the measurement campaign the 62.7% of winds blow from III and IV quadrants, whereas the 89.2% of winds had a speed <6 m/s. Furthermore, the period December 2019-February 2020 is mostly characterized by winds from northern I-IV quadrants, whereas the period April-August 2020 shows a dominant wind frequency from the southern II-III quadrants (not shown).

The daily-average wind speed and direction values were then calculated for the effective days (Fig. 5b) of PM monitoring using our device. The average-daily wind speed varies in the range 1.5–7.0 m/s (average 3.2 m/s) and can be classified in the following clusters: (i) L1 is 24%, (ii) L2 is 51.2%, (iii) L3 is 18.4% and (iv) L4 is 6.4%. Concerning wind provenance, the percentages for the I, II, III and IV quadrants are 14.4%, 20.0%, 28.0% and 37.6%, respectively. Using a wind-rose diagram (Fig. 5b) it is possible to observe that near half (45%) of the measured winds are blowing from two specific windows: a NW-window (N 306–337°, IV quadrant) and an S-window (N 179–196°, II-III quadrants) corresponding to the 27.2% and 12.8% of wind data, respectively.

When the daily average wind data are integrated to the daily average PM values (Fig. 6a–c) the following considerations are possible: (i) PM_{10} peaks >40 $\mu g/m^3$ are the 27.2% of total PM_{10} measures, $PM_{2.5}$ values >25 $\mu g/m^3$ are the 6.4% of total $PM_{2.5}$ data and PM_1 peaks in the range 6–12 $\mu g/m^3$ are the 12.0% of total PM_1 data; (ii) the winds blowing from the NW-window are associated with 12.8% of PM_{10} values >40 $\mu g/m^3$, 3.2% of $PM_{2.5}$ values >25 $\mu g/m^3$ and 4.8% of PM_1 peaks in the range 6–12 $\mu g/m^3$; (iii) none of those high PM values are associated to winds blowing from the S-window; and (iv) the few (4.8%) PM_1 values >12 $\mu g/m^3$ are invariably associated to a third western window (N 248-298°).

Interestingly, when also the RH is considered, it is possible to observe (Fig. 6d) how RH values were higher than 60% during the 76% of effective measurement days, with 16% of monitored days showing RH > 80%. Furthermore, the ca. 26% of days with RH > 60% are associated with winds blowing from the NW-window and with $PM_{2.5}$ an PM_{10} peaks. On the opposite, the winds from the S-window are generally characterized by lower (<60%) RH values.

In a preliminary source-to-sink approach, the integration of (i) the position of the used device within the southern area of the port (Fig. 1b), (ii) the relationship between the PM values and the wind characteristics so far discussed, and (iii) the existence of two

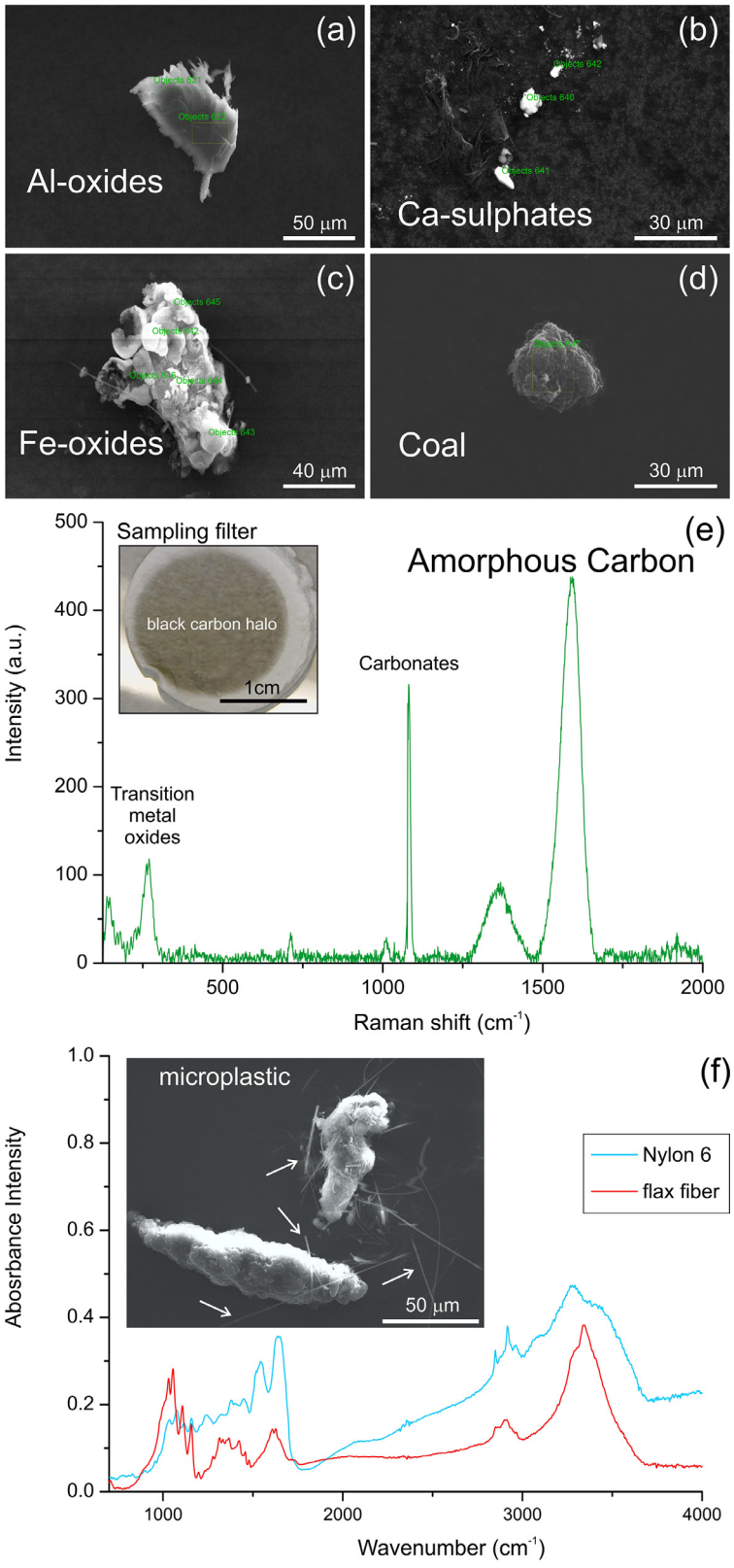

Fig. 4. (a–d) Coupled secondary electrons (SE) and back-scattered electrons (BSE) images for the most representative sampled airborne materials. (e) a representative Raman-spectroscopy spectrum highlighting the presence of amorphous carbon in the collected filters (inset of Fig. 4e). (f) Selected FT-IR spectrum and SE + BSE image (in the inset) of suspended microplastic fibers (indicated by white arrows in the inset image) in the sampled airborne micropollutants.

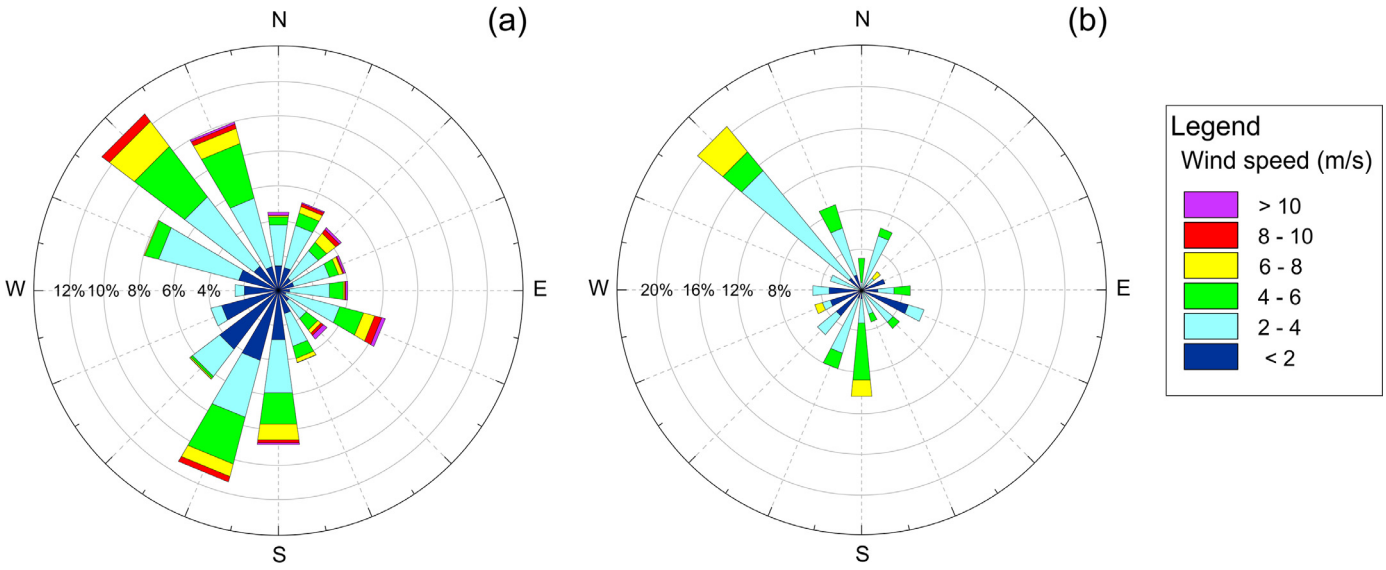

Fig. 5. Wind rose plot in the Port of Civitavecchia during (a) the whole test campaign and (b) the effective monitored days.

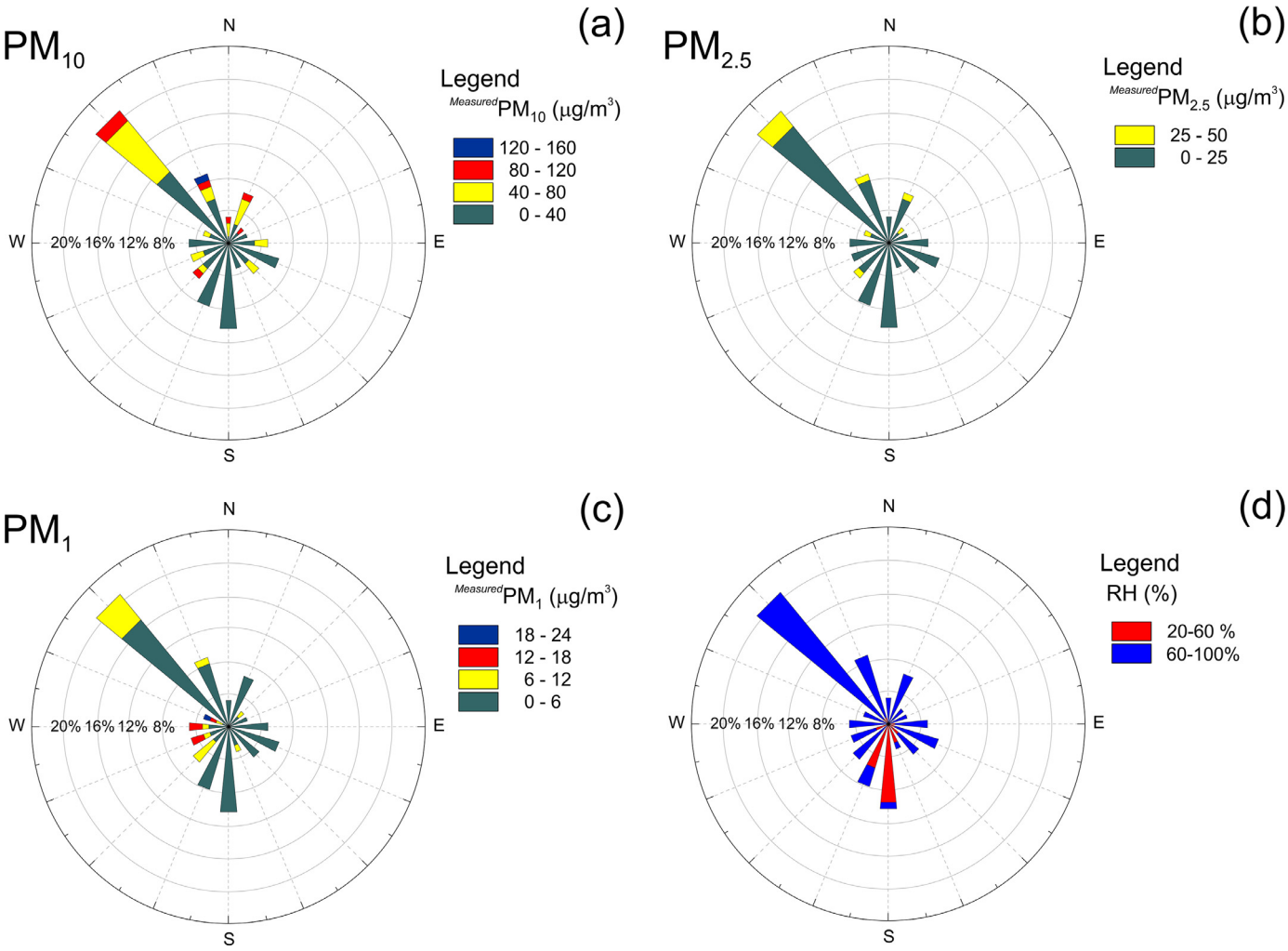

Fig. 6. Wind speed (radial) axes and polar contribution to the measured airborne (a) PM_{10}, (b) $PM_{2.5}$, (c) PM_1 and (d) relative humidity (RH) concentrations.

main windows for wind directions, allow us to make some working hypotheses on the main source areas for the airborne PM. In particular, the $PM_{2.5}$ and PM_{10} values associated with winds blowing from the S-window can be related to PM generated by the anthropic activities in the city of Civitavecchia located south to the device location. On the opposite, the high PM_1, $PM_{2.5}$ and PM_{10} values associated with winds from the NW-window could be related to PM material transported from the piers and from the two thermoelectric plants (TVN and Tirreno Power) to the S/SE area of the port where the OPC device is installed.

The common finding of black carbon particles (Fig. 4d) and carbon film coating (Fig. 4e) the filters, allows us to hypothesize marine diesel engines (Di Natale and Carotenuto, 2015; Gobbi et al., 2020) and the coal-fired power plants as main pollution sources (Zhang et al., 2005).

Concerning the highest PM_1 values, these are related to winds blowing from the sea (e.g., west), and therefore they could be interpreted as sea spray aerosol (Partanen et al., 2014). However, a precise defining of the source-to-sink relationships were far beyond the scope of this manuscript, and these working hypotheses need to be further investigated and verified.

4.2. Low-cost device vs. certified air quality monitoring stations

The daily average PM_{10} and $PM_{2.5}$ concentrations (raw data) detected by our device show trends comparable to those obtained from the ARPA Lazio monitoring stations (Fig. 7). To note, the PM_{10} (Fig. 7a) and $PM_{2.5}$ (Fig. 7b) intensities measured by the OPC–N3 are generally higher than those from the certified ARPA Lazio stations. Such a discrepancy between the OPC sensor based on light scattering technique (Sousan et al., 2016) and a referenced station based on inertial impactor gravimetric method (Zhu et al., 2007) has already been examined in several existing studies. Crilley et al. (2018, 2020) demonstrated that the disagreement appears to be primarily dependent on the ambient relative humidity (RH%); in the study area more than 70% of days had RH > 60%. When the ambient RH data are considered within the bi-variate comparisons between the OPC-based device and the ARPA Lazio stations (PM_{10} in Fig. 8 and $PM_{2.5}$ in Fig. 9), we note: (i) an evident loss of correlation for OPC values higher than >25 $\mu g/m^3$ and >10 $\mu g/m^3$ (values hereafter referred as thresholds) for PM_{10} and $PM_{2.5}$, respectively, with the OPC–N3 invariably over-estimating the PM concentrations; (ii) the OPC values exceeding these thresholds are always associated with high (60–88%) RH; (iii) for OPC values lower than the thresholds there is a good linear correlation with referenced ARPA Lazio stations, however the OPC–N3 seems to generally under-estimate the PM contents. Finally, (iv) the OPC values lower than the thresholds are associated with highly variable (25–82%) RH values.

To mathematically evaluate the divergence between the data from the OPC sensor and from the selected ARPA Lazio referenced stations, we developed an analysis of variance (ANOVA). Concerning the whole PM_{10} values, the results obtained from the regression analyses show acceptable *F*-test values (<0.05) only for five ARPA stations (i.e., n°15, n°60, n°103, n°104 and n°105) that can be considered therefore statistically significant. But low *R* (0.21–0.66) and R^2 (0.04–0.43) are invariably obtained for these five stations, suggesting very poor linear relationships.

Concerning the $PM_{2.5}$, *F*-test invariably show values >0.05 indicating a lack of statistical significance between the data from ARPA instruments and our low-cost device. We replicated then, the statistical analysis of variance only for the OPC concentrations lower than the threshold values. Regression analysis for PM_{10} < 25 $\mu g/m^3$ is always statistically significant (*F*-test < 0.05) for all the seven considered ARPA Lazio stations. Imposing the 0 intercept (i.e., testing the 1:1 hypothesis), the *R* and the R^2 values ranging between 0.87–0.94 and 0.76–0.89, respectively, indicate a significant positive linear relationship between the PM_{10} data obtained via the OPC and the referenced instruments from ARPA Lazio network. This relationship can be expressed as follow:

$$^{ARPA}PM_{10} = a*^{OPC}PM_{10}(\pm S.E.) \quad (4)$$

where *a* is the gradient of the linear regression (or ratio of the covariance) varying between 1.087–1.786 (average 1.370) and *S.E.* is the standard error derived by the statistical analysis and varying between ±6–14 $\mu g/m^3$ (average ±8 $\mu g/m^3$).

The regression analysis for $PM_{2.5}$ < 10 $\mu g/m^3$ is statistically significant, indicating a positive linear relationship:

$$^{ARPA}PM_{2.5} = a*^{OPC}PM_{2.5}(\pm S.E.) \quad (5)$$

characterized by *R* 0.87–0.93, R^2 0.76–0.87 and *a* 0.001–1.796 and *S.E.* ±3–5 $\mu g/m^3$.

Overall, the proposed analysis shows that for PM values lower than the thresholds, the data provided by the OPC–N3 counter and the referenced ARPA Lazio instruments are nicely correlated (R^2 > 0.76). However, the significant deviation from the 1:1 linear relationship, expected for two instruments monitoring the same phenomenon in the same area, suggests cautionary evaluation of these results.

Following the procedure by Crilley et al. (2018), the PM_{10} data from the optical particle counter was corrected to the local RH values. To perform this correction, we explored the existing relationship between the particle hygroscopicity and the volume, through the hygroscopicity parameter *k*. However, defining the *k* parameter, in this work, required to carefully consider the boundary conditions characterizing the studied data-set and the Civitavecchia area: (i) PM_{10} contents < threshold are related to highly variable RH values and to winds from both NW- and S-windows, (ii) PM_{10} contents > thresholds are invariably associated with high RH values and winds from the NW-window, and (iii) variable OPC–N3 sensor performances (under-estimates vs. over-estimates) in response to the different PM_{10} and RH values.

These boundary conditions are addressed here by using a sub population-based correction approach. Through the best-fitting method, graphically presented in the humidograms of Fig. 10a,b, we calculated two *k* parameters, one for PM_{10} ⟨ threshold and one for PM_{10} ⟩ threshold, hereafter indicated as *kLT* and *kHT*, respectively. The obtained *kLT* is 0.20 and it falls within the 0.36 ± 0.16 expected range for Europe (e.g., Pringle et al., 2010) and within the 0.3 ± 0.1 values for continental regions (Andreae and Rosenfeld, 2008). The calculated *kHT* shows instead higher value (0.61) however it is still within the typical range 0.1 < k< 0.9 for particulate matter (Fitzgerald et al., 1982; Hudson and Da, 1996; Dusek et al., 2006; Petters and Kreidenweis, 2007).

The obtained corrected PM_{10} values from the OP counter range between 3 and 62 $\mu g/m^3$. These values are in good agreement with the referenced ARPA Lazio "Porto" station, as also highlighted by a new analysis of variance (*F*-test < 0.05, intercept 0, *R* 0.84, R^2 0.71, slope *a* 0.8064, *S.E.* ±10 $\mu g/m^3$) and graphically shown in Fig. 10c. A better agreement is also evident with respect to all the time series of reported PM_{10} mass concentrations from all the seven referenced ARPA Lazio stations in Civitavecchia (Fig. 10d). Overall, the obtained results confirm previous findings (Holstius et al., 2014; Crilley et al., 2018, 2020; Di Antonio et al., 2018) regarding the impactful role of aerosol hygroscopicity in the correction and precise evaluation of PM concentrations measured using devices like OPCs. However, our case study outlines that the use of *k* parameters from the literature or locally derived *k* values cannot be completely appropriate for areas where the meteorological parameters (e.g., wind + RH) are extremely variable and have a strong role in controlling the airborne PM transportation and

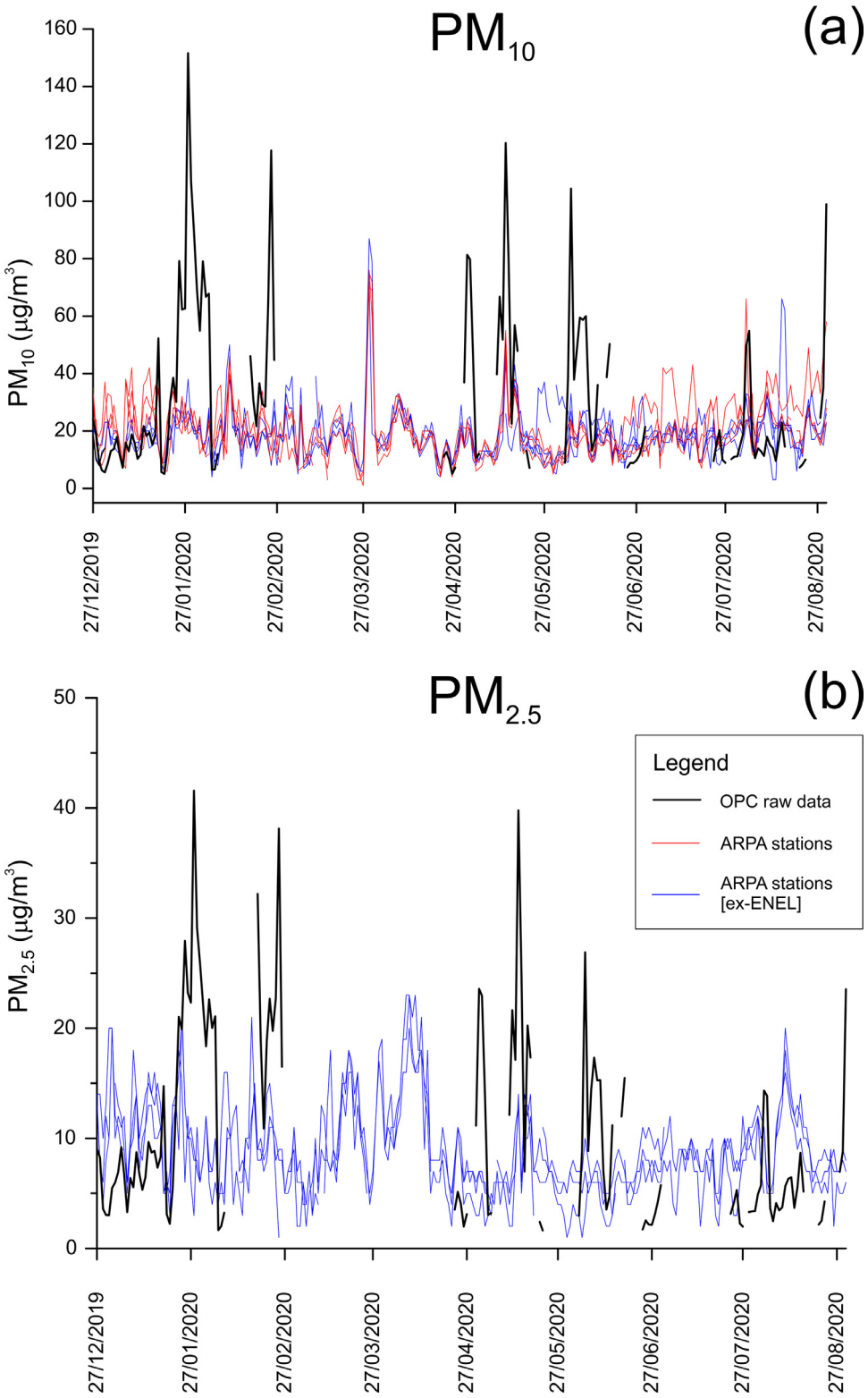

Fig. 7. Time series of the daily average (a) PM_{10} and (b) $PM_{2.5}$ concentrations measured by the OPC-equipped low-cost device (black pattern) and by governmental ARPA Lazio air quality monitoring stations (red and blue patterns).

concentrations. Moreover, our data show for the first time that a proper correction of the PM concentration yielded by OP counters is needed also for low (<60%) RH conditions. Further studies, however, are required to explore and better constrain this latter point that is crucial for the use of low-cost devices in highly anthropized areas.

4.3. A test for airborne PM monitoring during COVID-19 lockdown in Italy

On the 9th of March 2020, the Italian government decreed a full lockdown (the so-called "Phase-1″; Fig. 3), an unprecedented restrictive measure, to contrast the spreading of the severe acute

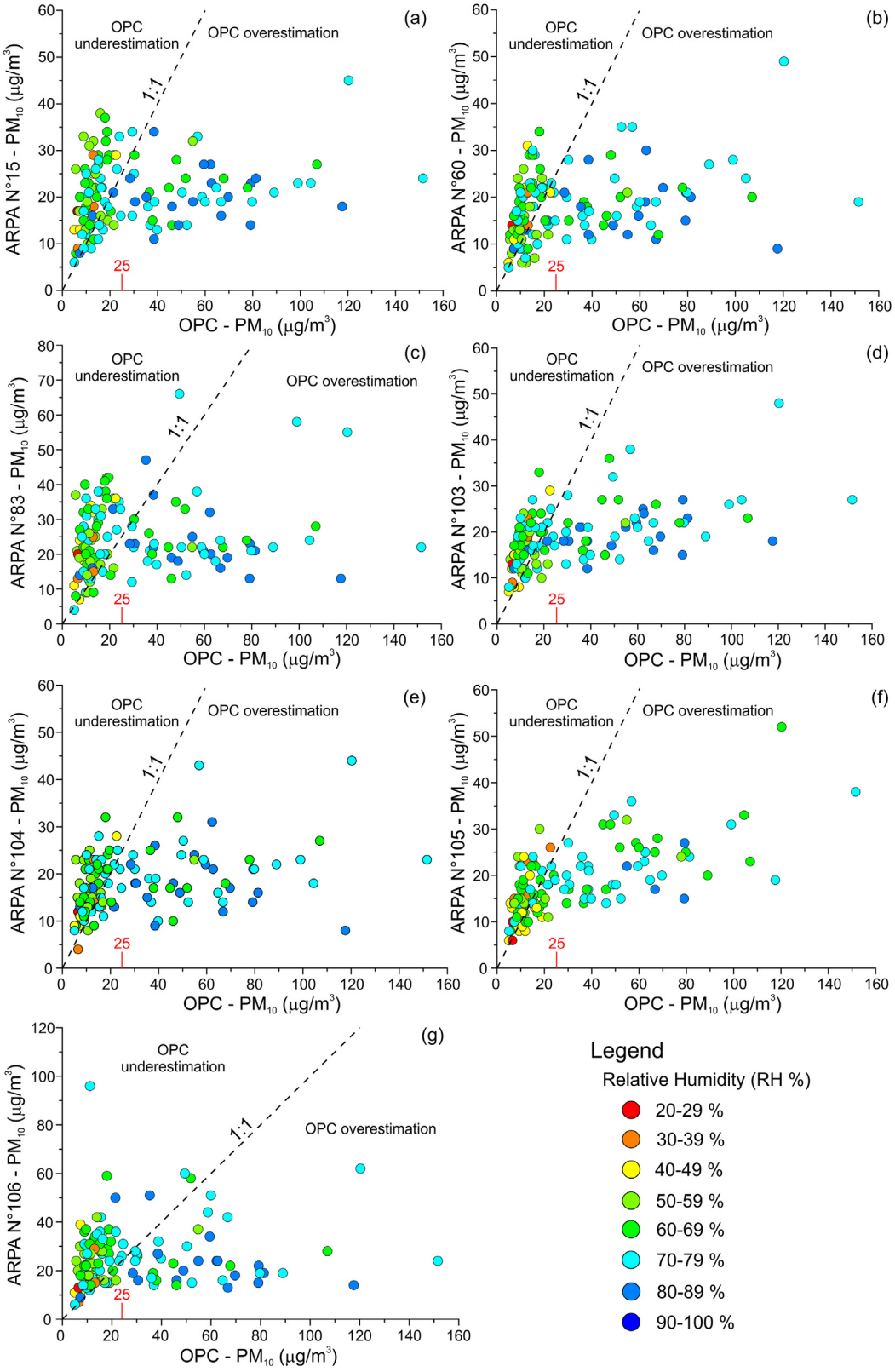

Fig. 8. (a–g) Uncorrected PM_{10} mass concentrations obtained from OPC–N3 plotted against data from ARPA Lazio monitoring stations; the data points are colored as a function of ambient RH. The line of 1:1 relationship between the two measuring systems is indicated. The performances (underestimation vs overestimation) of the OPC–N3 sensor with respect to ARPA Lazio referenced instruments and identified threshold value are also shown in red.

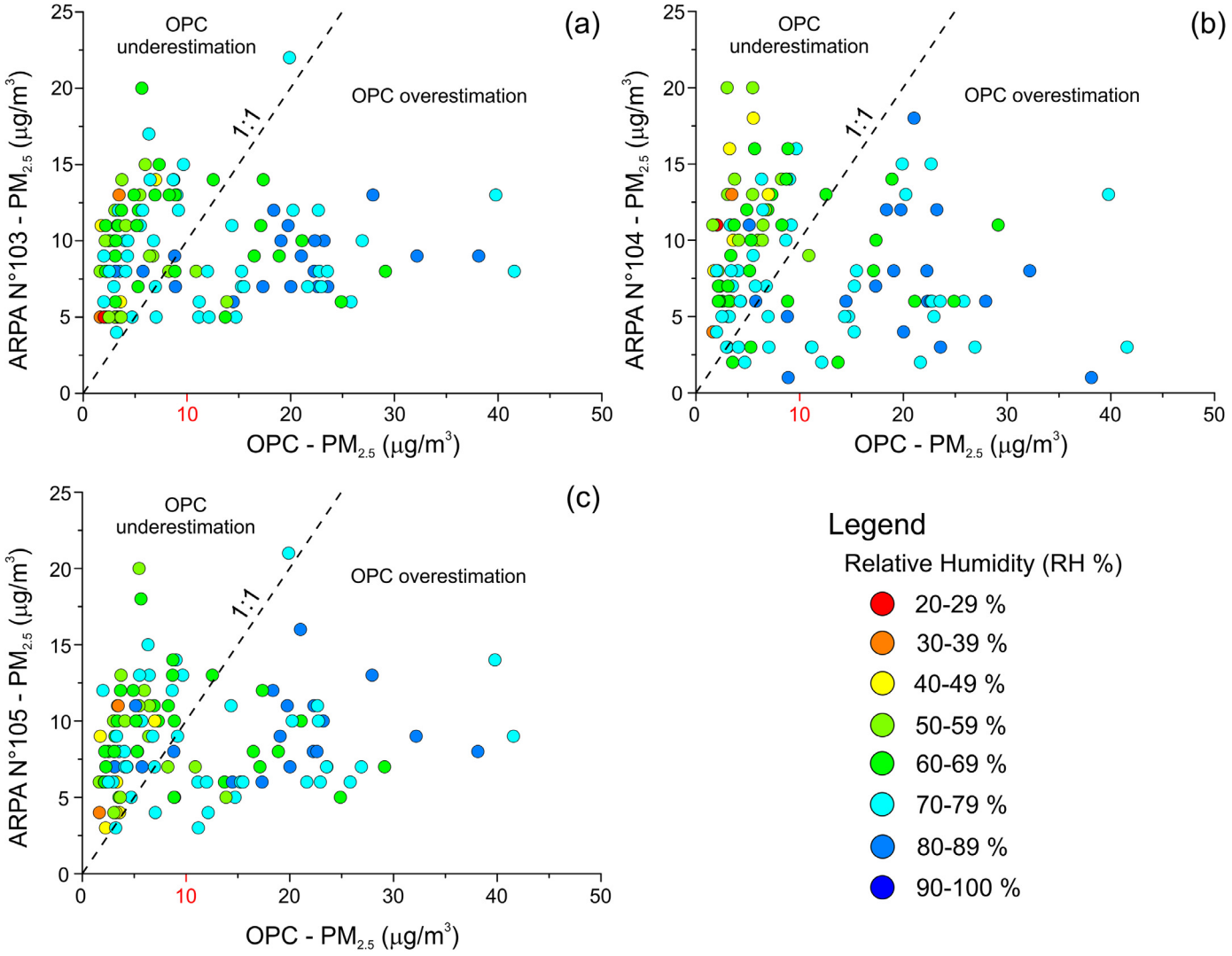

Fig. 9. (a–c) Uncorrected $PM_{2.5}$ mass concentrations obtained from OPC–N3 plotted against data from ARPA Lazio monitoring stations; the data points are colored as a function of ambient RH. The line of 1:1 relationship between the two measuring systems is indicated. The performances (underestimation vs overestimation) of the OPC–N3 sensor with respect to ARPA Lazio referenced instruments and identified threshold value are also shown in red.

respiratory syndrome coronavirus 2 (SARS-COV-2; e.g., Zhu et al., 2020) responsible for the COVID-19 pandemic. The full lockdown aimed at imposing physical distancing through the suspension of nonessential activities, banning social events, individual movement restrictions, school closures, rigid quarantine strategy, and reduction of both international and internal flights. Italian citizens were allowed to leave home only in specific circumstances (e.g., food and pharmacy shopping, medical needs, essential jobs). Italy was the first western country to experience a severe spreading of the SARS-COV-2, and the first non-Asian country to adopt a full lockdown strategy (Rugani and Caro, 2020; Marziano et al., 2021and references therein). The transition to lesser restrictive rules (so-called "Phase-2″) started the 3rd of May with reopening of strategic activities relevant for the Italian economy up to the lifting of the lockdown on the 18th of May.

The ten days from 24th of April to 3rd of May just before the ending of Phase 1 are characterized by the Liberation Day (April the 25th) and the Workers' Day (May the 1st) holidays. The celebrations for these two holidays are generally represented by short tourism trips, daily trips, moving to family country-houses or participating to mass gathering events such as "the 1st of May Concert" in Rome.

In 2019, the year before the COVID-19 pandemic, the Liberation Day corresponded to a longer weekend (25th to 28th of April) whereas the 1st of May occurred as a mid-week holiday. Inspection of the PM_{10} data collected during those days (blue pattern in Fig. 11) by the ARPA Lazio network in Civitavecchia, in Fiumicino (n°86 "Fiumicino Porto" and n°87 "Fiumicino Villa Guglielmi"; Supplementary Data, Fig. S1) and in Rome (n°39 "Villa Ada" and n°40 "Castel di Guido", representative of the city center and periphery, respectively; Supplementary Data, Fig. S1) shows a significant and expected spike (>100 $\mu g/m^3$) for the Liberation Day holiday and a minor one (up to 15 $\mu g/m^3$) for the Workers' Day holiday.

In 2020, these two holidays both corresponded to longer weekends (24th-26th of April and 1st–3rd of May, respectively) but occurring during the COVID-19 full lockdown period. While government restrictions were mostly respected during the Liberation Day holiday, the same was not true for the Workers' Day holiday, as reported by many Italian national and local newspapers; this is well documented by the PM_{10} concentrations from ARPA Lazio network (pink pattern in Fig. 11) characterized by (i) a flat profile for the Liberation Day and (ii) higher values (up to 25–30 $\mu g/m^3$) during the Workers' Day.

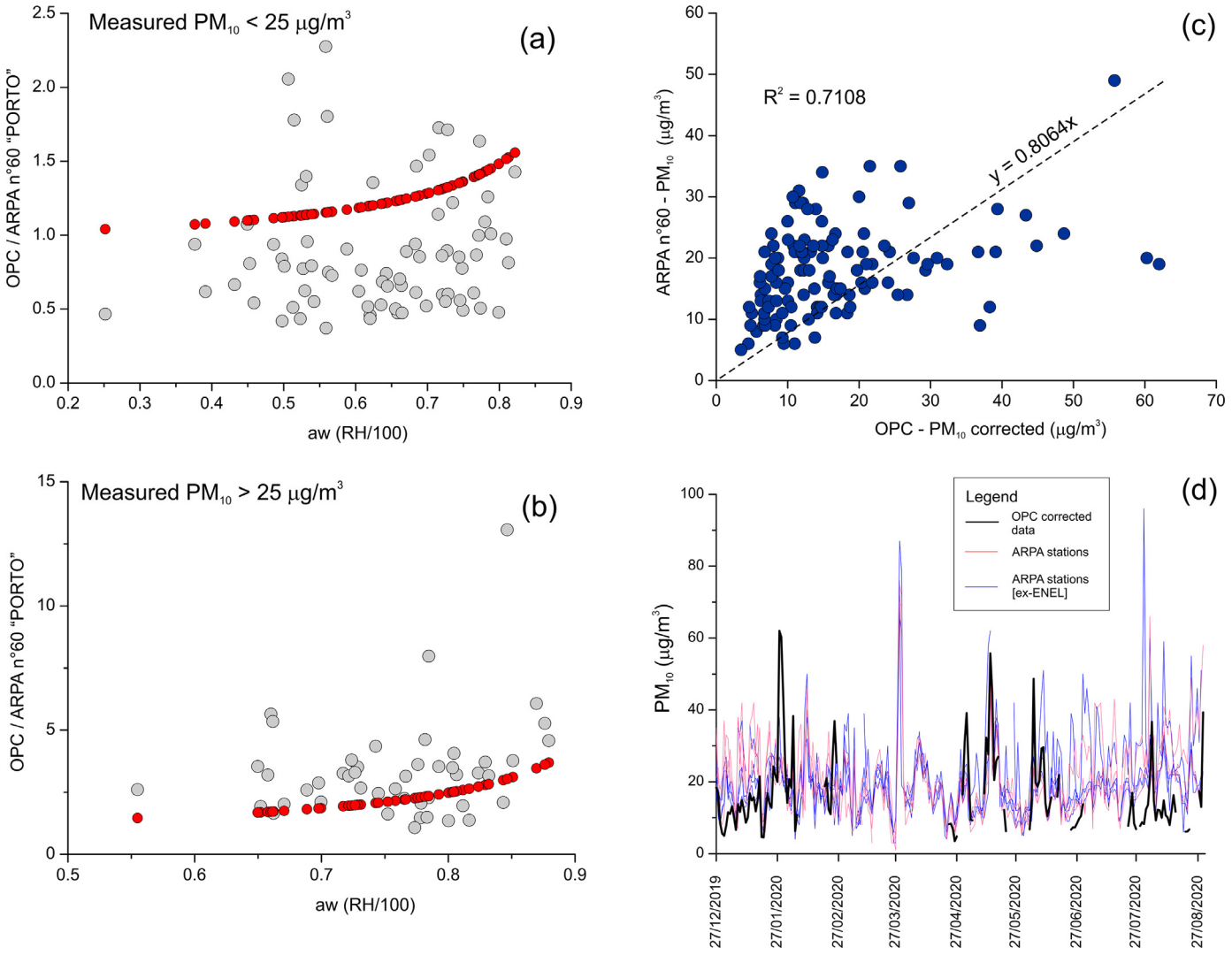

Fig. 10. Humidograms with the corresponding k fit (in red) for (a) measured PM_{10} < 25 mg/m^3 and (b) PM_{10} > 25 mg/m^3. (c) Scatterplot of corrected (see text for details) PM_{10} measurements from OPC–N3 vs. referenced ARPA Lazio N°60 station. (d) Time series of the daily average corrected PM_{10} concentrations obtained by the OPC-equipped low-cost device (black pattern) with respect to the governmental ARPA Lazio air quality monitoring stations (red and blue patterns).

A further relevant divergence between the 2019 and the 2020 PM_{10} patterns is the well-evident positive anomaly (up to 60–70 μg/m^3) registered in 2020 during the period 13th–18th of May and corresponding to the approaching to the lifting of the lockdown and the progressive reopening of commercial activities on 18th of May. To note, during the remaining days, the PM_{10} patterns for 2019 and 2020 overlap, in line with recent studies (Donzelli et al., 2020; Cameletti, 2020) highlighting the lack of a clear relationship between the full lockdown measures and the reduction of PM emission in urbanized areas.

Examining now the raw data from the OPC sensor (Fig. 3), we note for all PM fractions (PM_{10}, $PM_{2.5}$ and PM_1) the absence of peaks during the Liberation Day holiday whereas positive anomalies are recorded during both the Workers' Day weekend and at the lifting of the full lockdown restrictions. Furthermore, when comparing the corrected OPC PM_{10} mass concentrations (black line in Fig. 11) to the data from the ARPA Lazio network, we observe a perfect agreement between the OPC and the ARPA Lazio 2020 pattern.

Overall, the tested OPC-based device demonstrated to be effective in identifying events of severe airborne PM emission through the simple evaluation of raw data. When corrected for the meteorological background conditions, using the mathematical procedure set up during this work, it demonstrated to produce results comparable to referenced instruments.

4.4. Final remarks

The Port of Civitavecchia, located north to Roma, is one of the most important maritime hubs of the Mediterranean Sea, thus representing a valuable laboratory to test and develop next generation low-cost devices for monitoring and sampling the airborne particulate. We can summarize hereafter the significant outcomes of our work:

(i) The device installed in the southern area of the Port, during an eight-month campaign demonstrated to be able to monitor and coherently measure in real time the airborne PM_{10}, $PM_{2.5}$ and PM_1 mass fractions. The developed sampling system also permitted to collect a highly variable population of airborne material for laboratory characterization.

(ii) Optical, SEM-EDS and Raman characterization of the airborne sampled material showed the presence of Al-Fe-oxides, silicates, carbonates, and sulfates; most of the analyzed particles

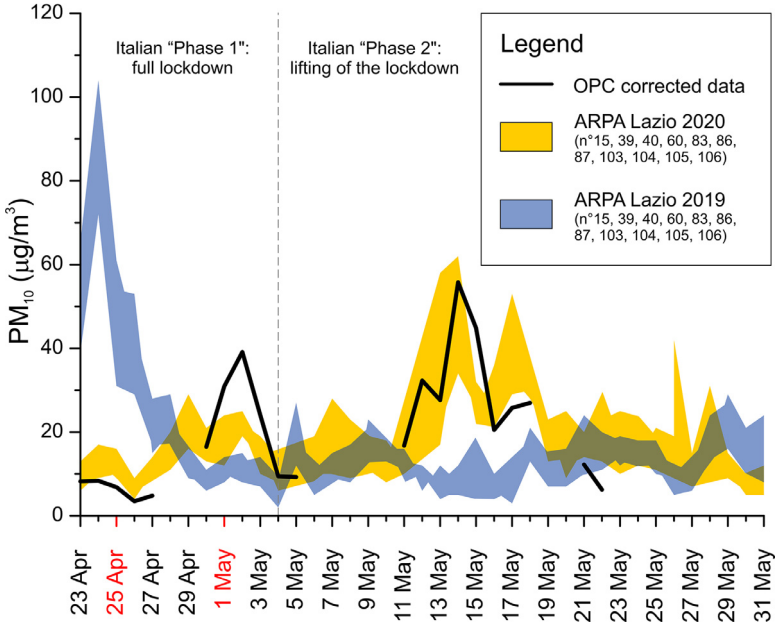

Fig. 11. Daily average corrected PM_{10} concentrations measured by the OPC-equipped low-cost device (black pattern) compared with the governmental ARPA Lazio data for the 2020 (yellow pattern) and for the 2019 (blue patterns) years. The peak of PM_{10} emissions during middle May 2020 corresponds to the transition from the COVID-19 full lockdown ("Phase-1″) to a progressive reopening of essential activities ("Phase-2″).

were found to be coated by thin films of amorphous carbon material. Based on the existing literature, these characteristics are comparable to PM emitted from maritime diesel engines and coal-fueled plants.

(iii) FT-IR investigations outlined the presence of airborne microplastics in the form of nylon and flax fibers. This impactful finding confirms the recent literature on the high dispersion of microplastics in the whole environment.

(iv) The integration of wind data to PM characteristics (concentrations and types) permitted a preliminary source-to-sink approach with the identification of two main PM sources: a main NW-source related to the docks and two thermoelectric plants, responsible for the majority of PM_{10} and $PM_{2.5}$, and a second source possibly corresponding to the town of Civitavecchia.

(v) The analysis of variance developed for evaluating the relationship between PM data from the OPC device and the referenced ARPA Lazio monitoring stations confirmed the necessity to correct the PM raw data from the OPC-based device for the local RH conditions. The ANOVA also evidenced for the first time, irrespective to the RH, that the - OPC-N3 systematically under-estimates PM concentration for $PM_{10} < 25\ \mu g/m^3$ and $PM_{2.5} < 10\ \mu g/m^3$, and over-estimates PM values for concentrations higher than these thresholds.

(vi) The PM_{10} mass correction relative to the nearest ARPA Lazio station was modeled following the *k*-Kohler theory but considering the threshold values identified in this work. The resulting corrected PM_{10} concentrations are statistically in good agreement with the referenced data from the ARPA Lazio network.

(vii) The OPC-based device was able to correctly monitor, during the month of May 2020, the PM punctuated anomalies related to the lifting of the full lockdown adopted by the Italian Government to contrast the COVID-19 pandemic.

In conclusion, the results obtained during this study provide compelling evidence for the valuable contribution of low-cost OPC sensors in developing up-to-date airborne PM monitoring strategies.

5. Conclusion

There is a general consensus that strongly urbanized coastal regions represent air pollution factories, with the anthropogenic-derived emissions increasingly recognized as a major global threat affecting the whole ecosystems and representing the very-next challenge for preserving the natural environment and the human health. This challenge requires to update the air quality monitoring strategies. To contribute to this global quest, we designed a low-cost device (ca. 1000 €) capable to measure the particulate matter (PM) concentrations via an optical particle counter (OPC) and simultaneously sampling it via standard 2.5 cm filters for PM characterization through microscopy and spectroscopy techniques. These latter investigations identified in the study area for the first time the presence of airborne nylon and textile fibers, and therefore highlighted the dramatically increasing human exposure to microplastics.

Lastly, this study identified for the first time the existence of OPC-performance threshold values for measured PM ($\mu g/m^3$) strongly controlled by meteorological condition such as the ambient RH. This highlighted the necessity of a deeper and more complex data treatment and application of the k-Kohler theory for modeling and correcting the OPC raw data. Further work is however required to fully standardize the strategies for evaluating PM raw data and to test in different natural and anthropic environments.

Declaration of Competing Interest

The authors declare that they have no competing financial interests or personal relationships that could have appeared to influence the work reported in this paper.

Fundings

Funding for this work were provided by the Italian Presidenza del Consiglio dei Ministri (DARA) through the MIAMI and the Smart Mountain projects.

Data availability

The main data that support the findings of this study are included in this published article and its supplementary files. The complete datasets generated during and/or analysed during the current study are available from the corresponding authors on reasonable request.

CRediT authorship contribution statement

Federico Lucci: Writing – original draft, Conceptualization, Methodology, Validation, Data curation, Data curation. **Giancarlo Della Ventura:** Conceptualization, Methodology, Validation, Data curation, Writing – original draft, Supervision, Funding acquisition, Data curation. **Daniele Piazzolla:** Conceptualization, Methodology, Validation, Data curation, Writing – original draft, Data curation. **Carlo Venettacci:** Resources, Methodology, Software, Data curation. **Andrea Terribili:** Resources, Methodology, Software, Data curation. **Cecilia La Bella:** Formal analysis, Investigation, Formal analysis, Data curation. **Alessandra Conte:** Formal analysis, Investigation, Formal analysis, Data curation. **Simone Bonamano:** Formal analysis, Investigation, Data curation. **Sergio Scanu:** Formal analysis, Investigation, Data curation. **Francesco Radica:** Formal analysis, Investigation, Formal analysis, Data curation. **Marco Marcelli:** Formal analysis, Investigation, Data curation.

Acknowledgments

The constructive reviews of three anonymous reviewers as well the professional handling of the Editor Xiaofang He greatly contributed to improve the manuscript. FL gratefully acknowledges Prof. M. Santosh. The Grant to Department of Science, Roma Tre University (MIUR-Italy Dipartimenti di Eccellenza, ARTICOLO 958 1, COMMI 314–337 LEGGE 232/2016) is gratefully acknowledged. The authors thank the Environmental Office of the Port Authority System of the Central Northern Tyrrhenian Sea for supporting the implementation of the C–CEMS weather station with which the wind and humidity data used in this study were acquired.

Supplementary materials

Supplementary material associated with this article can be found, in the online version, at doi:10.1016/j.geogeo.2022.100120.

References

Adachi, K., Chung, S.H., Buseck, P.R., 2010. Shapes of soot aerosol particles and implications for their effects on climate. J. Geophys. Res. Atmos. 115 (D15). doi:10.1029/2009JD012868.

Agrawal, G., Mohan, D., Rahman, H., 2021. Ambient air pollution in selected small cities in India: observed trends and future challenges. IATSS Res. 45 (1), 19–30. doi:10.1016/j.iatssr.2021.03.004.

Andreae, M.O., Rosenfeld, D., 2008. Aerosol–cloud–precipitation interactions. Part 1. The nature and sources of cloud-active aerosols. Earth Sci. Rev. 89 (1–2), 13–41. doi:10.1016/j.earscirev.2008.03.001.

Bonamano, S., Piermattei, V., Madonia, A., Mendoza, F., Pierattini, A., Martellucci, R., Stefanì, G., Zappalà, G., Caruso, G., Marcelli, M., 2016. The Civitavecchia coastal environment monitoring system (C-CEMS): a new tool to analyze the conflicts between coastal pressures and sensitivity areas. Ocean Sci. 12 (1). doi:10.5194/os-12-87-2016.

Bonamano, S., Madonia, A., Piazzolla, D., Paladini de Mendoza, F., Piermattei, V., Scanu, S., Marcelli, M., 2017. Development of a predictive tool to support environmentally sustainable management in port basins. Water 9 (11), 898. doi:10.3390/w9110898, (Basel).

Brauer, M., Freedman, G., Frostad, J., et al., 2016. Ambient air pollution exposure estimation for the global burden of disease 2013. Environ. Sci. Technol. 50, 79–88. doi:10.1021/acs.est.5b03709.

Brunekreef, B., Forsberg, B., 2005. Epidemiological evidence of effects of coarse airborne particles on health. Eur. Respir. J. 26, 309–318. doi:10.1183/09031936.05.00001805.

Bunzl, K., Hotzl, H., Rosner, G., Winkler, R., 1984. Spatial distribution of radionuclides in soil around a coal-fired power plant: 210 Pb, 210Po, 226Ra, 232Th, 40 K emitted with the fly ash and 137Cs from the worldwide weapon testing fallout. Sci. Total Environ. 38, 15–31. doi:10.1016/0048-9697(84)90204-3.

Cafaro, V., Piazzolla, D., Melchiorri, C., Burgio, C., Fersini, G., Conversano, F., Piermattei, V., Marcelli, M., 2018. Underwater noise assessment outside harbor areas: the case of port of Civitavecchia, northern Tyrrhenian Sea, Italy. Mar. Pollut. Bull. 133, 865–871. doi:10.1016/j.marpolbul.2018.06.058.

Cameletti, M., 2020. The effect of Corona virus lockdown on air pollution: evidence from the city of Brescia in Lombardia region (Italy). Atmos. Environ. 239, 117794. doi:10.1016/j.atmosenv.2020.117794.

Carballo, T., Gil, M.V., Gómez, X., González-Andrés, F., Morán, A., 2008. Characterization of different compost extracts using Fourier-transform infrared spectroscopy (FTIR) and thermal analysis. Biodegradation 19 (6), 815–830. doi:10.1007/s10532-008-9184-4.

Cole, M., Lindeque, P., Halsband, C., Galloway, T.S., 2011. Microplastics as contaminants in the marine environment: a review. Mar. Pollut. Bull. 62, 2588–2597. doi:10.1016/j.marpolbul.2011.09.025.

Cowger, W., Steinmetz, Z., Gray, A., Munno, K., Lynch, J., Hapich, H., Primpke, S., De Frond, H., Rochman, C., Herodotou, O., 2021. Microplastic Spectral Classification Needs an Open Source Community: Open Specy to the Rescue!. Analytical Chemistry 93 (21), 7543–7548. doi:10.1021/acs.analchem.1c00123.

Crilley, L.R., Shaw, M., Pound, R., Kramer, L.J., Price, R., Young, S., Lewis, A.C., Pope, F.D., 2018. Evaluation of a low-cost optical particle counter (Alphasense OPC-N2) for ambient air monitoring. Atmos. Meas. Tech. Discuss. doi:10.5194/amt-2017-308.

Crilley, L.R., Singh, A., Kramer, L.J., Shaw, M.D., Alam, M.S., Apte, J.S., Bloss, W.J., Hildebrandt Ruiz, L., Fu, P., Fu, W., Gani, S., Gatari, M., Ilyinskaya, E., Lewis, A.C., Ng'ang'a, D., Sun, Y., Whitty, R.C.W., Yue, S., Young, S., Pope, F.D., 2020. Effect of aerosol composition on the performance of low-cost optical particle counter correction factors. Atmos. Meas. Tech. 13 (3), 1181–1193. doi:10.5194/amt-13-1181-2020.

Della Ventura, G., Gozzi, F., Marcelli, A., 2017. In: The MIAMI Project: Design and Testing of an IoT Lowcost Device for Mobile Monitoring of PM and Gaseous Pollutants, 12. Superstripe Press, pp. 41–44 Science Series.

De Nazelle, A., Bode, O., Orjuela, J.P., 2017. Comparison of air pollution exposures in active vs. passive travel modes in European cities: a quantitative review. Environ. Int. 99, 151–160. doi:10.1016/j.envint.2016.12.023.

Di Antonio, A., Popoola, O.A., Ouyang, B., Saffell, J., Jones, R.L., 2018. Developing a relative humidity correction for low-cost sensors measuring ambient particulate matter. Sensors 18 (9), 2790. doi:10.3390/s18092790.

Di Natale, F., Carotenuto, C., 2015. Particulate matter in marine diesel engines exhausts: emissions and control strategies. Transportation Research Part D: Transport and Environment 40, 166–191. doi:10.1016/j.trd.2015.08.011.

Dong, Z., Kang, S., Qin, D., Shao, Y., Ulbrich, S., Qin, X., 2018. Variability in individual particle structure and mixing states between the glacier–snowpack and atmosphere in the northeastern Tibetan Plateau. Cryosphere 12 (12), 3877–3890. doi:10.5194/tc-12-3877-2018.

Dong, Z., Qin, D., Li, K., Kang, S., Wei, T., Lu, J., 2019. Spatial variability, mixing states and composition of various haze particles in atmosphere during winter and summertime in northwest China. Environ. Pollut. 246, 79–88. doi:10.1016/j.envpol.2018.11.101.

Donzelli, G., Cioni, L., Cancellieri, M., Llopis Morales, A., Morales Suárez-Varela, M.M., 2020. The effect of the COVID-19 lockdown on air quality in three Italian medium-sized cities. Atmosphere 11 (10), 1118. doi:10.3390/atmos11101118, (Basel).

Dusek, U., Frank, G.P., Hildebrandt, L., Curtius, J., Schneider, J., Walter, S., Chad, D., Drewnick, F., Hings, S., Jung, D., Borrmann, S., Andreae, M.O., 2006. Size matters more than chemistry for cloud-nucleating ability of aerosol particles. Science 312 (5778), 1375–1378. doi:10.1126/science.1125261.

Elminir, H.K., 2005. Dependence of urban air pollutants on meteorology. Sci. Total Environ. 350 (1–3), 225–237. doi:10.1016/j.scitotenv.2005.01.043.

Enyoh, C.E., Verla, A.W., Verla, E.N., Ibe, F.C., Amaobi, C.E., 2019. Airborne microplastics: a review study on method for analysis, occurrence, movement and risks. Environ. Monit. Assess. 191 (11), 1–17. doi:10.1007/s10661-019-7842-0.

European Environment Agency, 2020. Air Quality in Europe: 2020 Report. Publications Office of the European Union, Luxembourg doi:10.2800/786656.

Fitzgerald, J.W., Hoppel, W.A., Vietti, M.A., 1982. The size and scattering coefficient of urban aerosol particles at Washington, DC as a function of relative humidity. J. Atmos. Sci. 39 (8), 1838–1852. doi:10.1175/1520-0469(1982)039<1838:TSASCO>2.0.CO;2.

Gao, S., Cong, Z., Yu, H., Sun, Y., Mao, J., Zhang, H., … Bai, Z., 2019. Estimation of background concentration of PM in Beijing using a statistical integrated approach. Atmos. Pollut. Res. 10 (3), 858–867. doi:10.1016/j.apr.2018.12.014.

Gobbi, G.P., Di Liberto, L., Barnaba, F., 2020. Impact of port emissions on EU-regulated and non-regulated air quality indicators: the case of Civitavecchia (Italy). Sci. Total Environ. 719, 134984. doi:10.1016/j.scitotenv.2019.134984.

Gozzi, F., Della Ventura, G., Marcelli, A., 2015. Mobile monitoring of particulate matter: state of art and perspectives. Atmos. Pollut. Res. 7, 228–234. doi:10.1016/j.apr.2015.09.007.

Gozzi, F., Della Ventura, G., Marcelli, A., Lucci, F., 2017. Current status of particulate matter pollution in Europe and future perspectives: a review. J. Mater. Environ. Sci. 8 (6), 1901–1909 ISSN 2028-2508.

Grantz, D.A., Garner, J.H.B., Johnson, D.W., 2003. Ecological effects of particulate matter. Environ. Int. 29, 213–239. doi:10.1016/S0160-4120(02)00181-2.

Guerra, S.A., Lane, D.D., Marotz, G.A., Carter, R.E., Hohl, C.M., Baldauf, R.W., 2006. Effects of wind direction on coarse and fine particulate matter concentrations

in southeast Kansas. J. Air Waste Manag. Assoc. 56, 1525–1531. doi:10.1080/10473289.2006.10464559.
Guo, S., Hu, M., Zamora, M.L., Peng, J., Shang, D., Zheng, J., Du, Z., Wu, Z., Shao, M., Zeng, L., Molina, M.J., Zhang, R., 2014. Elucidating severe urban haze formation in China. Proc. Natl. Acad. Sci. 111 (49), 17373–17378. doi:10.1073/pnas.1419604111.
Holstius, D.M., Pillarisetti, A., Smith, K.R., Seto, E., 2014. Field calibrations of a low-cost aerosolsensor at a regulatory monitoring site in California. Atmos. Meas. Tech. 7, 1121–1131. doi:10.5194/amt-7-1121-2014, 2014.
Horemans, B., Cardell, C., Bencs, L., Kontozova-Deutsch, V., De Wael, K., Van Grieken, R., 2011. Evaluation of airborne particles at the Alhambra monument in Granada, Spain. Microchem. J. 99 (2), 429–438. doi:10.1016/j.microc.2011.06.018.
Hu, M., Wang, Y., Wang, S., Jiao, M., Huang, G., Xia, B., 2021. Spatial-temporal heterogeneity of air pollution and its relationship with meteorological factors in the Pearl River Delta, China. Atmos. Environ. 254, 1–14. doi:10.1016/j.atmosenv.2021.118415, 118415.
Huang, R.J., Zhang, Y., Bozzetti, C., et al., 2014. High secondary aerosol contribution to particulate pollution during haze events in China. Nature 514, 218–222. doi:10.1038/nature13774.
Huang, Y., Qing, X., Wang, W., Han, G., Wang, J., 2020. Mini-review on current studies of airborne microplastics: analytical methods, occurrence, sources, fate and potential risk to human beings. TrAC Trends Anal. Chem. 125, 115821.
Hudson, J.G., Da, X., 1996. Volatility and size of cloud condensation nuclei. J. Geophys. Res. Atmos. 101 (D2), 4435–4442. doi:10.1029/95JD00192.
Institute for Health Metrics and Evaluation (IHME), 2018. Findings from the Global Burden of Disease Study 2017. IHME, Seattle, Lancet, WA.
Jacob, D.J., Winner, D.A., 2009. Effect of climate change on air quality. Atmos. Environ. 43, 51–63. doi:10.1016/j.atmosenv.2008.09.051.
Jenks, G.F., 1967. The data model concept in statistical mapping. International Yearbook of Cartography, 7. Bertelsmann Verlag, pp. 186–190.
Jerrett, M., Donaire-Gonzalez, D., Popoola, O., Jones, R., Cohen, R.C., Almanza, E., de Nazelle, A., Mead, I., Carrasco-Turigas, G., Cole-Hunter, T., Triguero-Mas, M., Seto, E., Nieuwenhuijsen, M., 2017. Validating novel air pollution sensors to improve exposure estimates for epidemiological analyses and citizen science. Environ. Res. 158, 286–294. doi:10.1016/j.envres.2017.04.023.
Kamińska, J.A., 2018. The use of random forests in modelling short-term air pollution effects based on traffic and meteorological conditions: a case study in Wrocław. J. Environ. Manag. 217, 164–174. doi:10.1016/j.jenvman.2018.03.094.
Kavak Akpinar, E., Akpinar, S., Oztop, H.F., 2006. Effects of meteorological parameters on air pollutant concentrations in Elazig, Turkey. Int. J. Green Energy 3 (4), 407–421. doi:10.1080/01971520600873392.
Kgabi, N.A., Pienaar, J.J., Kulmala, M., 2008. Characterisation of inhalable atmospheric aerosols. WIT Trans. Ecol. Environ. 116, 323–333.
Khaniabadi, Y. O., Sicard, P., Khaniabadi, A. O., Mohammadinejad, S., Keishams, F., Takdsatan, A., Najafi, A., De Marco, A., Daryanoosh, M., 2018. Air quality modeling for health risk assessment of ambient PM10, PM2. 5 and SO2 in Iran. Human and Ecological Risk Assessment: An International Journal 25 (5), 1298–1310. doi:10.1080/10807039.2018.1487277.
Kumar, P., Hama, S., Nogueira, T., Abbass, R. A., Brand, V. S., de Fatima Andrade, M., Asfaw, A., Hama Aziz, K., Cao, S., El-Gendy, A., Islam, S., Jeba, F., Khare, M., Mamuya, S. H., Martinez, J., Meng, M., Morawska, L., Muula, A. S., Shiva Nagendra, S. M., Ngowi, A. V., Omer, K., Olaya, Y., Osano, P., Salam, A., 2021. In-car particulate matter exposure across ten global cities. Science of the total environment 750, 141395. doi:10.1016/j.scitotenv.2020.141395.
Kumar, P., Morawska, L., Birmili, W., Paasonen, P., Hu, M., Kulmala, M., Harrison, R.M., Norford, L., Britter, R., 2014. Ultrafine particles in cities. Environ. Int. 66, 1–10. doi:10.1016/j.iatssr.2021.03.004.
Li, L., Qian, J., Ou, C.Q., Zhou, Y., Guo, C., Guo, Y., 2014. Spatial and temporal analysis of air pollution index and its timescale-dependent relationship with meteorological factors in Guangzhou, China, 2001–2011. Environ. Pollut. 190, 75–81. doi:10.1016/j.envpol.2014.03.020.
Li, H., Meier, F., Lee, X., Chakraborty, T., Liu, J., Schaap, M., Sodoudi, S., 2018. Interaction between urban heat island and urban pollution island during summer in Berlin. Sci. Total Environ. 636, 818–828.
Lucci, F., Rossetti, F., White, J.C., Moghadam, H.S., Shirzadi, A., Nasrabady, M., 2016. Tschermak fractionation in calc-alkaline magmas: the Eocene Sabzevar volcanism (NE Iran). Arabian J. Geosci. 9 (10), 573.
Lucci, F., Carrasco-Núñez, G., Rossetti, F., Theye, T., White, J.C., Urbani, S., Azizi, H., Asahara, Y., Giordano, G., 2020. Anatomy of the magmatic plumbing system of Los Humeros Caldera (Mexico): implications for geothermal systems. Solid Earth 11, 125–159. doi:10.5194/se-11-125-2020.
Martellucci, R., Salon, S., Cossarini, G., Piermattei, V., Marcelli, M., 2021. Coastal phytoplankton bloom dynamics in the Tyrrhenian sea: advantage of integrating *in situ* observations, large-scale analysis and forecast systems. J. Mar. Syst. 218, 103528. doi:10.1016/j.jmarsys.2021.103528.
Marziano, V., Guzzetta, G., Rondinone, B.M., Boccuni, F., Riccardo, F., Bella, A., Poletti, P., Trentini, F., Pezzotti, P., Brusaferro, S., Rezza, G., Iavicoli, S., Ajelli, M., Merler, S., 2021. Retrospective analysis of the Italian exit strategy from COVID-19 lockdown. Proc. Natl. Acad. Sci. 118 (4), e2019617118. doi:10.1073/pnas.2019617118.
Miccoli, A., Mancini, E., Saraceni, P.R., Della Ventura, G., Scapigliati, G., Picchietti, S., 2022. First evidence of *in vitro* cytotoxic effects of marine microlitter on Merluccius merluccius and Mullus barbatus, two Mediterranean commercial fish species. Sci. Total Environ. 813, 152618. doi:10.1016/j.scitotenv.2021.152618.
Minguillón, M.C., Querol, X., Baltensperger, U., Prévôt, A.S.H., 2012. Fine and coarse PM composition and sources in rural and urban sites in Switzerland: local or regional pollution? Sci. Total Environ. 427, 191–202.
Moghadam, H.S., Li, Q.L., Kirchenbaur, M., Garbe-Schonberg, D., Lucci, F., Griffin, W.L., Ghorbani, G., 2021. Geochemical and isotopic evolution of late oligocene magmatism in Quchan, NE Iran. Geochem. Geophys. Geosyst. 22. doi:10.1029/2021GC009973, ISSN: 1525-2027.
Mokadem, N., Hamed, Y., Sâad, A.B., Gargouri, I., 2014. Atmospheric pollution in North Africa (ecosystems–atmosphere interactions): a case study in the mining basin of El Guettar–M'Dilla (southwestern Tunisia). Arabian J. Geosci. 7 (5), 2071–2079. doi:10.1007/s12517-013-0852-2.
Nel, A., 2005. Atmosphere: enhanced: air pollution-related illness: effects of particles. Science 308, 804–806. doi:10.1126/science.1108752.
Papadimitriou, S., Lyridis, D.V., Koliousis, I.G., Tsioumas, V., Sdoukopoulos, E., Stavroulakis, P.J., 2018. Motorways of the sea'(MoS) and related european policies. In: The Dynamics of Short Sea Shipping. Palgrave Macmillan, Cham, pp. 119–161. doi:10.1007/978-3-319-98044-7_6 Palgrave Studies in Maritime Economics.
Partanen, A.I., Dunne, E.M., Bergman, T., Laakso, A., Kokkola, H., Ovadnevaite, J., Sogacheva, L., Baisnée, D., Sciare, J., Manders, A., O'Dowd, C., de Leeuw, G., Korhonen, H., 2014. Global modelling of direct and indirect effects of sea spray aerosol using a source function encapsulating wave state. Atmos. Chem. Phys. 14 (21), 11731–11752. doi:10.5194/acp-14-11731-2014.
Pearce, J.L., Beringer, J., Nicholls, N., Hyndmand, R.J., Tapper, R.J., 2011. Quantifying the influence of local meteorology on air quality using generalized additive models. Atmos. Environ. 45, 1328–1336. doi:10.1016/j.Atmos env.2010.11.051.
Petters, M.D., Kreidenweis, S.M., 2007. A single parameter representation of hygroscopic growth and cloud condensation nucleus activity. Atmos. Chem. Phys. 7 (8), 1961–1971. doi:10.5194/acp-7-1961-2007.
Peters, J., Theunis, J., Van Poppel, M., Berghmans, P., 2013. Monitoring PM10 and ultrafine particles in urban environments using mobile measurements. Aerosol Air Qual. Res. 13 (2), 509–522. doi:10.4209/aaqr.2012.06.0152.
Piazzolla, D., Cafaro, V., Mancini, E., Scanu, S., Bonamano, S., Marcelli, M., 2020a. Preliminary investigation of microlitter pollution in low-energy hydrodynamic basins using Sabella spallanzanii (Polychaeta: sabellidae) tubes. Bull. Environ. Contam. Toxicol. 104 (3), 345–350. doi:10.1007/s00128-020-02797-x.
Piazzolla, D., Cafaro, V., de Lucia, G.A., Mancin, I.E., Scanu, S., Bonamano, S., Piermattei, V., Vianello, A., Della Ventura, G., Marcelli, M., 2020b. Microlitter pollution in coastal sediments of the northern Tyrrhenian Sea, Italy: microplastics and fly-ash occurrence and distribution. Estuar. Coast. Shelf Sci. 241, 106819. doi:10.1016/j.ecss.2020.106819.
Piazzolla, D., Della Ventura, G., Terribili, A., Conte, A., Scanu, S., Bonamano, S., Marcelli, M., Lucci, F., La Bella, C., and Venettacci, C. (2021). Air pollution assessment using a cost-effective device: the case study of the northern Latium coastal area., EGU General Assembly 2021, online, 19–30 Apr 2021, EGU21-10223. DOI: 10.5194/egusphere-egu21-10223, 2021.
Piras, P., Maiorino, L., Teresi, L., Meloro, C., Lucci, F., Kotsakis, T., Raia, P., 2013. Bite of the cats: relationships between functional integration and mechanical performance as revealed by mandible geometry. Syst. Biol. 62 (6), 878–900.
Pope, F.D., Dennis-Smither, B.J., Griffiths, P.T., Clegg, S.L., Cox, R.A., 2010. Studies of single aerosol particles containing mal#onic acid, glutaric acid, and their mixtures with sodium chloride. I. Hygroscopic growth. J. Phys. Chem. A 114, 5335–5341. doi:10.1021/jp100059k.
Prata, J.C., 2018. Airborne microplastics: consequences to human health? Environ. Pollut. 234, 115–126.
Pringle, K.J., Tost, H., Pozzer, A., Pöschl, U., Lelieveld, J., 2010. Global distribution of the effective aerosol hygroscopicity parameter for CCN activation. Atmos. Chem. Phys. 10 (12), 5241–5255. doi:10.5194/acp-10-5241-2010.
Rugani, B., Caro, D., 2020. Impact of COVID-19 outbreak measures of lockdown on the Italian carbon footprint. Sci. Total Environ. 737, 139806. doi:10.1016/j.scitotenv.2020.139806.
Scanu, S., Soetebier, S., Piazzolla, D., Tiralongo, F., Mancini, E., Romano, N., Marcelli, M., 2015. Concentrations of As, Cd, Cr, Ni, and Pb in the echinoid paracentrotus lividus on the coast of Civitavecchia, northern Tyrrhenian Sea, Italy. Reg. Stud. Mar. Sci. 1, 7–17. doi:10.1016/j.rsma.2015.02.001.
Silva, L.F., Pinto, D., Neckel, A., Oliveira, M.L., Sampaio, C.H., 2020. Atmospheric nanocompounds on Lanzarote Island: vehicular exhaust and igneous geologic formation interactions. Chemosphere 254, 126822.
Soggiu, M.E., Inglessis, M., Gagliardi, R.V., Settimo, G., Marsili, G., Notardonato, I., Avino, P., 2020. PM10 and PM2. 5 qualitative source apportionment using selective wind direction sampling in a port-industrial area in Civitavecchia, Italy. Atmosphere 11 (1), 94. doi:10.3390/atmos11010094.
Sousan, S., Koehler, K., Hallett, L., Peters, T.M., 2016. Evaluation of the Alphasense optical particle counter (OPC-N2) and the Grimm portable aerosol spectrometer (PAS-1.108). Aerosol Sci. Technol. 50 (12), 1352–1365. doi:10.1080/02786826.2016.1232859.
Tian, G., Qiao, Z., Xu, X., 2014. Characteristics of particulate matter (PM10) and its relationship with meteorological factors during 2001–2012 in Beijing. Environ. Pollut. 192, 266–274. doi:10.1016/j.envpol.2014.04.036.
Thompson, J.E., 2016. Crowd-sourced air quality studies: a review of the literature & portable sensors. Trends Environ. Anal. Chem. 11, 23–34. doi:10.1016/j.teac.2016.06.001.
Trejos, E.M., Silva, L.F., Hower, J.C., Flores, E.M., González, C.M., Pachón, J.E., Aristizábal, B.H., 2021. Volcanic emissions and atmospheric pollution: a study of nanoparticles. Geosci. Front. 12 (2), 746–755. doi:10.1016/j.gsf.2020.08.013.

Tseng, D.Y., Vir, R., Traina, S.J., Chalmers, J.J., 1996. A fourier-transform infrared spectroscopic analysis of organic matter degradation in a bench-scale solid substrate fermentation (composting) system. Biotechnol. Bioeng. 52 (6), 661–671. doi:10.1002/(SICI)1097-0290(19961220)52:6<661::AID-BIT4>3.0.CO;2-M.

Van den Bossche, J., Peters, J., Verwaeren, J., Botteldooren, D., Theunis, J., De Baets, B., 2015. Mobile monitoring for mapping spatial variation in urban air quality: development and validation of a methodology based on an extensive dataset. Atmos. Environ. 105, 148–161. doi:10.1016/j.atmosenv.2015.01.017.

Wang, Z., Cheng, Y., Ma, N., Mikhailov, E., Pöschl, U., Su, H., 2017. Dependence of the hygroscopicity parameter κ on particle size, humidity and solute concentration: implications for laboratory experiments, field measurements and model studies. Atmos. Chem. Phys. Discuss. 2017, 1–33. doi:10.5194/acp-2017-253.

Zhang, C., Yao, Q., Sun, J., 2005. Characteristics of particulate matter from emissions of four typical coal-fired power plants in China. Fuel Process. Technol. 86 (7), 757–768. doi:10.1016/j.fuproc.2004.08.006.

Zhang, H., Wang, Y., Hu, J., et al., 2015. Relationships between meteorological parameters and criteria air pollutants in three megacities in China. Environ. Res. 140, 242–254. doi:10.1016/j.Envres.2015.04.004.

Zhang, B., Jiao, L., Xu, G., Zhao, S., Tang, X., Zhou, Y., Gong, C., 2018. Influences of wind and precipitation on different-sized particulate matter concentrations (PM 2.5, PM 10, PM 2.5–10). Meteorol. Atmos. Phys. 130 (3), 383–392.

Wang, H., Nie, L., Li, J., Wang, Y., Wang, G., Wang, J., Hao, Z., 2013. Characterization and assessment of volatile organic compounds (VOCs) emissions from typical industries. Chinese Science Bulletin 58 (7), 724–730. doi:10.1007/s11434-012-5345-2.

Zeb, B., Alam, K., Sorooshian, A., Blaschke, T., Ahmad, I., Shahid, I., 2018. On the morphology and composition of particulate matter in an urban environment. Aerosol Air Qual. Res. 18 (6), 1431. doi:10.4209/aaqr.2017.09.0340.

Zhou, W., Tie, X., Zhou, G., Liang, P., 2015. Possible effects of climate change of wind on aerosol variation during winter in Shanghai, China. Particuology 20, 80–88. doi:10.1016/j.partic.2014.08.008.

Zhu, K., Zhang, J., Lioy, P.J., 2007. Evaluation and comparison of continuous fine particulate matter monitors for measurement of ambient aerosols. J. Air Waste Manag. Assoc. 57 (12), 1499–1506. doi:10.3155/1047-3289.57.12.1499.

Zhu, N., Zhang, D., Wang, W., Li, X., Yang, B., Song, J., Zhao, X., Huang, B., Shi, W., Lu, R., Niu, P., Zhan, F., Ma, X., Wang, D., Xu, W., Wu, G., Gao, G.F., Phil, D., Tan, W., 2020. A novel coronavirus from patients with pneumonia in China, 2019. N. Engl. J. Med. 382, 727–733. doi:10.1056/NEJMoa2001017.